Comput. Methods Appl. Mech. Engrg. 267 (2013) 293–317

Contents lists available at ScienceDirect

Comput. Methods Appl. Mech. Engrg.

journal homepage: www.elsevier.com/locate/cma

# The use of updated robust reliability measures in stochastic dynamical systems

H.A. Jensen [a,*], C. Vergara [a], C. Papadimitriou [b], E. Millas [a]

[a] Department of Civil Engineering, Santa Maria University, Valparaiso, Chile
[b] Department of Mechanical Engineering, University of Thessaly, GR-38334 Volos, Greece

ARTICLE INFO

*Article history:*
Received 5 March 2013
Received in revised form 5 July 2013
Accepted 25 August 2013
Available online 5 September 2013

*Keyword:*
Bayesian updating
First-excursion probability
Robust reliability
Simulation methods
Structural reliability

ABSTRACT

This work explores the effect of using updated robust reliability measures in the context of stochastic structural dynamical systems. A Bayesian probabilistic methodology for model updating is first implemented for the purpose of updating the structural model using dynamic data. The updated distribution of the system model parameters is then used to implement a strategy for updating the system reliability. The effect of the updated information on the robust performance and design of dynamical systems under stochastic excitation and modeling uncertainty is illustrated by several example problems.



## 1. Introduction

During operation conditions structural systems may deteriorate for a number of reasons, such as fatigue, corrosion, damage induced in structural elements by strong wind loads or earthquakes, etc. These conditions may lead to significant reduction of the structural reliability. Therefore, the re-assessment of the reliability of a structure after it has been built by monitoring the dynamic response is of paramount importance [1–4]. The updated reliability may be used to identify potentially unsafe structures, to schedule repairs, maintenances or inspection intervals, or to design retrofitting or control strategies [5–9]. For a proper assessment of the updated reliability all uncertainties affecting the structural safety should be considered. This leads to the concept of robust reliability defined in [10], and used in this work, to take into account during reliability estimation the structural modeling uncertainties in addition to the uncertain excitation that a structure will experience during its lifetime. Using a probabilistic description of these uncertainties the concept of updated robust reliability can be defined in terms of an integral over a specified set of possible models of the conditional reliability for a given model weighted by the probability of that model [11,12].

In this work a strategy for updating robust structural reliability using dynamic data is first considered. For this purpose, a Bayesian probabilistic framework for model updating is integrated with advanced simulation tools [13]. The model identification technique provides more accurate representations of the uncertainties associated with the structural modeling because it is based on both measured data and prior engineering information. In particular, a multi-level Markov chain Monte Carlo algorithm is adopted here [14]. In this framework, revised information about the uncertainties in the system parameters is obtained, which is expressed by posterior probability density functions. It is noted that in this context probability is not interpreted in the usual frequentist sense, but it is based on the idea of reasonable expectation, that is, probability is

* Corresponding author. Tel.: +56 32 2654383; fax: +56 32 2654115.
*E-mail address:* hector.jensen@usm.cl (H.A. Jensen).

0045-7825/$ - see front matter © 2013 Elsevier B.V. All rights reserved.
http://dx.doi.org/10.1016/j.cma.2013.08.015

interpreted as a measure of plausibility of the hypothesis. In this manner, it is possible to extend the application of probability theory to problems where the frequentist interpretation may not be directly intuitive. Using this interpretation, Bayesian approach makes it possible to deal with usual situations in structural engineering where a large amount of experimental data is not available, and it provides a means for making decisions based on limited and incomplete information [15]. Using the updated characterization of the system model, a strategy is implemented for computing the reliability of structural systems under future excitations characterized by means of stochastic processes. In this context, the probability that design conditions are satisfied within a particular reference period is used as reliability measure. Such measure is referred as the first excursion probability and quantifies the plausibility of the occurrence of unacceptable behavior of the structural system [16–18]. The strategy is based on subset simulation and it uses a Markov chain Monte Carlo technique based on the Metropolis algorithm for generating conditional samples [19,20].

Using the proposed strategy for updating the robust structural reliability, it is the main objective of this contribution to investigate the effect of the updated information on the robust performance and design of dynamical systems under stochastic excitation and modeling uncertainty. The proposed study is illustrated by considering several problems involving structure-related applications. The structure of the paper is as follows. Section 2 reviews some of the basic ideas of Bayesian updating using dynamic data. The reliability assessment of structural systems under stochastic excitation is examined in Section 3. The proposed implementation for updating the reliability estimation is introduced in Section 4. The effect of using updated reliability measures is illustrated in Section 5 by means of three application problems. The paper closes with some conclusions and final remarks.

## 2. Bayesian updating using dynamic data

### 2.1. Problem definition

In this section a Bayesian approach for model updating using input–output measurements is briefly reviewed. The methodology is based on a probabilistic system identification approach introduced in [21,22]. The approach allows for the explicit treatment of the uncertainties arising from both measurement noise and modeling errors by providing a probabilistic description of the structural models and the prediction error for each structural model from a prescribed class of models. It also allows for the explicit treatment of non-uniqueness arising in the model updating inverse problem. Let $M$ be the assumed probabilistic model class for a target system, parameterized by the vector of uncertain model parameters $\boldsymbol{\theta} \in \Theta \subset R^{n_p}$, and $D$ be the measured dynamic data from the system. The objective of Bayesian model updating is to define the posterior probability density function of $\boldsymbol{\theta}$ conditioned on $D, p(\boldsymbol{\theta}|M, D)$, as (Bayes' Theorem) [13,23]

$$p(\boldsymbol{\theta}|M, D) = \frac{p(D|M, \boldsymbol{\theta})\ p(\boldsymbol{\theta}|M)}{p(D|M)}, \tag{1}$$

where $p(\boldsymbol{\theta}|M)$ is the initial (prior) probability density function of $\boldsymbol{\theta}, p(D|M, \boldsymbol{\theta})$ is the likelihood function, and $p(D|M)$ is the evidence of $M$. The prior probability distribution reflects the relative plausibility of each model in the model class $M$ before utilizing the data $D$. The term $p(D|M, \boldsymbol{\theta})$ gives the probability of obtaining the data $D$ based on the model $M$ specified by the parameters $\boldsymbol{\theta}$. Finally, the normalizing constant $p(D|M)$, which does not affect the shape of the posterior distribution, corresponds to the evidence for the model class $M$ given by the data $D$, and expressed as

$$p(D|M) = \int_{\Theta} p(D|M, \boldsymbol{\theta})\ p(\boldsymbol{\theta}|M) d\boldsymbol{\theta}. \tag{2}$$

As previously pointed out only one probabilistic model class $M$ for a target system, defined by the parameters $\boldsymbol{\theta}$, is considered in the present formulation. Therefore the problem of model class selection, among candidate probabilistic model classes, is not taken into account here [11,14].

### 2.2. Formulation of likelihood function

The likelihood function gives a measure of the agreement between the system response and the corresponding structural model output. This measure of the data fit of each model in the model class $M$, i.e., the value of the likelihood function for each parameter vector $\boldsymbol{\theta}$, is given by the probability model established for the system output. This can be constructed by choosing a probability model for the prediction error, which is the difference between the system output that will be measured and the one predicted by the structural model for a specified value of the parameter vector $\boldsymbol{\theta}$. Let $\mathbf{x}(t_n, \boldsymbol{\theta})$ be the model response vector at $N$ degrees of freedom at time $t_n = n\Delta t, n = 1, \ldots, N_t$, where $\Delta t$ denotes the sampling time step and $N_t$ is the number of available data. The input for calculating the model response is assumed to be prescribed. Because of measurement noise and modeling error (prediction error), the measured response $\mathbf{y}(t_n)$ at $N_o, (N_o \leqslant N)$ observed degrees of freedom of the structural model will differ from the model response $\mathbf{B}_o\mathbf{x}(t_n, \boldsymbol{\theta})$. This last term corresponds to the measured degrees of freedom where $\mathbf{B}_o$ denotes an $N_o \times N$ observation matrix. This matrix selects only those degrees of freedom where measurements are made. The probability model class for the prediction error $\mathbf{e}(t_n, \boldsymbol{\theta}) = \mathbf{y}(t_n) - \mathbf{B}_o\mathbf{x}(t_n, \boldsymbol{\theta})$ considered in the present formulation is based on the maximum entropy principle which yields a multi-dimensional Gaussian distribution with zero

mean and covariance matrix $\mathbf{\Sigma}_e$ [10,24,25]. This distribution arises because it gives the largest amount of uncertainty among all probability distributions for a real variable whose first two moments are specified [26]. In particular, the prediction error $\mathbf{e}(t_n, \boldsymbol{\theta})$ is modeled as a discrete zero mean Gaussian white noise process, that is,

$$E[\mathbf{e}(t_n, \boldsymbol{\theta})] = 0, \quad E[\mathbf{e}(t_n, \boldsymbol{\theta})\mathbf{e}(t_m, \boldsymbol{\theta})^T] = \mathbf{\Sigma}_e \, \delta_{nm}, \tag{3}$$

where $E[\cdot]$ denotes expectation, $\delta_{nm}$ denotes the kronecker delta function, and $\mathbf{\Sigma}_e$ denotes the $N_o \times N_o$ covariance matrix which is assumed to have the form $\mathbf{\Sigma}_e = \sigma_e^2 \mathbf{I}_o$, where $\mathbf{I}_o$ is the identity matrix of dimension $N_o \times N_o$. This assumption implies equal variances and stochastic independence of the prediction errors for different channels of measurements. Of course, different prediction error model classes can be used as well. Using the above probability model for the prediction error it can be shown that the likelihood function $p(D|M, \boldsymbol{\theta})$ can be expressed in terms of a measure-of-fit function $J(\boldsymbol{\theta}|M, D)$ between the measured response and the model response at the measured degrees of freedom [10,21,22,25]. Such function is given by

$$J(\boldsymbol{\theta}|M, D) = \frac{1}{N_t N_o} \sum_{n=1}^{N_t} \|\mathbf{y}(t_n) - \mathbf{B}_o \mathbf{x}(t_n, \boldsymbol{\theta})\|^2 \tag{4}$$

where $\|\cdot\|$ denotes the Euclidian norm of a vector.

### 2.3. Model parameters

For a large number of available data ($N_t N_0$ is large) it has been found that the most probable model parameters $\hat{\boldsymbol{\theta}}$ are obtained by minimizing $J(\boldsymbol{\theta}|M, D)$ over all parameters in $\Theta$ that it depends on [21]. Recall that the parameter vector $\boldsymbol{\theta}$ for identification includes parameters such as structural parameters and the prediction error variance. Under the assumption of a large amount of data the posterior probability density function $p(\boldsymbol{\theta}|M, D)$ is in general concentrated in the neighborhood of a lower dimensional manifold in the parameter space. If the dimension is zero there may be a unique optimal parameter (global identifiable case), or a discrete set of optimal parameters (local identifiable case) [27–29]. On the other hand, if the dimension is larger than zero the number of optimal solutions may be either infinity (strictly unidentifiable case) or it may be finite but the decay of the distribution in the vicinity of the various optimal points may not be rapid enough in all directions (almost unidentifiable case) [30,31]. In the latter case the vicinities of important probabilities corresponding to different optimal points may either overlap or they may extend over larger regions. In this case the manifold in the neighborhood of which all points with significant probabilities are contained is of dimension larger than zero extending along the directions of the parameter space where the probability density function decays slowly. All points along the manifold correspond to structural models that have almost the same response at the measured degrees of freedom to within the accuracy specified by the optimal prediction variance $\hat{\sigma}^2 = J(\hat{\boldsymbol{\theta}}|M.D)$ [10,21].

### 2.4. Simulation-based methods

As indicated before one of the difficulties of model updating is that the problem is potentially ill-posed, that is, there may be more than one optimal solution. The problem becomes even more challenging when only some degrees of freedom of the model are measured and when modeling errors are explicitly considered. Bayesian model updating approaches reported in [21,22] have been successfully used in resolving the aforementioned difficulties when the posterior probability density function of the model parameters is very peaked (identifiable cases). In those cases asymptotic approximations of the Bayesian predictive integrals can be used with sufficient accuracy [10,32]. However, when the probability density function is not very peaked, i.e., when the amount of data is limited or the probability density function has a flat region, the validity of the asymptotic approximations is doubtful. To avoid the above difficulties a simulation-based Bayesian model updating technique is adopted here. In general, simulation-based methods can handle more general cases than asymptotic approximation approaches [11]. In particular, an efficient method called transitional Markov chain Monte Carlo is implemented in this work [14]. Validation calculations have shown the effectiveness of this approach in a series of practical Bayesian model updating problems [14,33,34]. The method can be applied to a wide range of cases including high-dimensional posterior probability density functions, multimodal distributions, peaked probability density functions, and probability density functions with flat regions.

### 2.5. Transitional Markov chain Monte Carlo method

For completeness the basic ideas of the transitional Markov chain Monte Carlo method are presented in this section. The method iteratively proceeds from the prior to the posterior distribution. It starts with the generation of samples from the prior distribution in order to populate the space in which also the most probable region of the posterior distribution lies. For this purpose a number of intermediate distributions are defined as

$$p_j(\boldsymbol{\theta}|M, D) = c \, p(\boldsymbol{\theta}|M) p(D|M, \boldsymbol{\theta})^{\alpha_j} \; j = 0, 1, \ldots, m, \quad 0 = \alpha_0 < \alpha_1 < \cdots < \alpha_m = 1, \tag{5}$$

where the index $j$ denotes the step number, and $c$ is a normalizing constant. The exponent $\alpha_j$ can be interpreted as the percentage of the total information provided by the dynamic data which is incorporated in the $j$th iteration of the updating procedure. The first step ($j = 0$) corresponds to the prior distribution and in the last stage ($j = m$) the samples are generated from the posterior distribution. The idea is to choose the values of exponents $\alpha_j$ in such a way that the change of the shape between two adjacent intermediate distributions be small. This small change of the shape makes it possible to efficiently obtain samples from $p_{j+1}(\boldsymbol{\theta}|M,D)$ based on the samples from $p_j(\boldsymbol{\theta}|M,D)$. The samples are obtained by generating Markov chains where the lead samples are selected from the distribution $p_j(\boldsymbol{\theta}|M,D)$ by computing their plausibility weights with respect to $p_{j+1}(\boldsymbol{\theta}|M,D)$ which are given by

$$w(\boldsymbol{\theta}_j^k) = \frac{p(\boldsymbol{\theta}_j^k|M)\; p(D|M,\boldsymbol{\theta}_j^k)^{\alpha_{j+1}}}{p(\boldsymbol{\theta}_j^k|M)\; p(D|M,\boldsymbol{\theta}_j^k)^{\alpha_j}} = p(D|M,\boldsymbol{\theta}_j^k)^{\alpha_{j+1}-\alpha_j}, \quad k = 0,1,\ldots,N_j, \tag{6}$$

where the upper index $k = 1,\ldots,N_j$ denotes the sample number in the $j$th iteration step ($\boldsymbol{\theta}_j^k, k = 1,\ldots,N_j$). Each sample of the current stage is generating using the Metropolis–Hastings algorithm [19,20]. The starting point of the Markov chain is a sample from the previous step that is selected according to the probability equal to its normalized weight

$$\bar{w}(\boldsymbol{\theta}_j^k) = \frac{w(\boldsymbol{\theta}_j^k)}{\sum_{l=1}^{N_j} w(\boldsymbol{\theta}_j^l)}, \quad k = 1,\ldots,N_j. \tag{7}$$

The proposal probability density function for the Metropolis–Hastings algorithm is a Gaussian distribution centered at the preceding sample of the chain and with a covariance matrix $\boldsymbol{\Sigma}_j$ equal to the scaled version of the estimated covariance matrix of the current intermediate distribution, that is

$$\boldsymbol{\Sigma}_j = \beta^2 \sum_{l=1}^{N_j} \bar{w}(\boldsymbol{\theta}_j^l)\left[(\boldsymbol{\theta}_j^l - \bar{\boldsymbol{\theta}}_j)(\boldsymbol{\theta}_j^l - \bar{\boldsymbol{\theta}}_j)^T\right], \quad \bar{\boldsymbol{\theta}}_j = \sum_{l=1}^{N_j} \bar{w}(\boldsymbol{\theta}_j^l)\boldsymbol{\theta}_j^l, \tag{8}$$

where $\beta^2$ is a scaling parameter that is used to control the rejection rate of the Metropolis–Hastings algorithm and to smooth the Markov chain Monte Carlo jumps. As previously pointed out, one of the key aspects of the method is the smooth transition between two adjacent intermediate distributions. In this regard, the degree of uniformity of the plausibility weights $w(\boldsymbol{\theta}_j^k), k = 1,\ldots,N_j$ is a good indicator of how close $p_{j+1}(\boldsymbol{\theta}|M,D)$ is to $p_j(\boldsymbol{\theta}|M,D)$. Thus, to ensure the smooth transition between iterations the parameter $\alpha_j$ is chosen so that the coefficient of variation of the plausibility weights is smaller or equal to a prescribed threshold, that is $\sigma_{wj}|E_{wj} \leqslant \gamma$, where

$$\sigma_{wj}^2 = \frac{1}{N_j - 1}\sum_{l=1}^{N_j}\left[p(D|M,\boldsymbol{\theta}_j^l)^{\alpha_{j+1}-\alpha_j} - E_{wj}\right]^2, \quad E_{wj} = \frac{1}{N_j}\sum_{l=1}^{N_j} p(D|M,\boldsymbol{\theta}_j^l)^{\alpha_{j+1}-\alpha_j}. \tag{9}$$

The previous steps are repeated until $\alpha_j = 1$ is reached (samples generated from the posterior distribution). At the last stage the samples ($\boldsymbol{\theta}_m^k, k = 1,\ldots,N_m$) are asymptotically distributed as $p(\boldsymbol{\theta}|M,D)$. For a detailed implementation of the transitional Markov chain Monte Carlo method the reader is referred to [14,35].

## 3. System reliability

### 3.1. Reliability measure

The updating procedure presented in the previous section is now used to update the system reliability. As previously pointed out, the focus is in stochastic structural dynamical systems where the reliability is defined in terms of a first excursion probability, that is the probability that design conditions are satisfied within a particular reference period. In this context, a failure domain $F$ can be defined as

$$F(M) = \{\mathbf{q}^T =< \mathbf{z}^T, \boldsymbol{\theta}^T > |d(\mathbf{q}|M) > 1\} \tag{10}$$

where $\mathbf{z}$ represents the vector of random variables that specify the stochastic excitation, $\mathbf{q}$ denotes the augmented vector of system parameters (loading and model parameters), and

$$d(\mathbf{q}|M) = \max_{j=1,\ldots,n_j}\max_{t\in[0,T]}\frac{|r_j(t,\mathbf{z},\boldsymbol{\theta})|}{r_j^*}, \tag{11}$$

indicates the normalized demand function, where $[0,T]$ is the time interval of analysis, $r_j(t,\mathbf{z},\boldsymbol{\theta}), j = 1,\ldots,n_j$ are the response functions associated with the failure event that defines the failure domain $F$, and $r_j^*$ is the corresponding critical threshold level. The response functions $r_j(t,\mathbf{z},\boldsymbol{\theta}), j = 1,\ldots,n_j$ are obtained from the solution of the equation of motion that characterizes the structural model.

### 3.2. Nominal and robust failure probability

The probability of the failure event associated with the failure domain $F$ predicted using known model parameters $\boldsymbol{\theta}$ is referred as the nominal or conditional failure probability, and it can be expressed as

$$P(F|M,\boldsymbol{\theta}) = \int_{\Omega_z} \Pi_F(\mathbf{z},\boldsymbol{\theta}|M)\, f(\mathbf{z})\, d\mathbf{z}, \tag{12}$$

where $\Pi_F(\mathbf{z},\boldsymbol{\theta}|M)$ is the indicator function, that is, $\Pi_F(\mathbf{z},\boldsymbol{\theta}|M) = 1$ if $(\mathbf{z},\boldsymbol{\theta}|M) \in F$ and $\Pi_F(\mathbf{z},\boldsymbol{\theta}|M) = 0$ otherwise. The vector of random variables that specify the excitation is characterized by a probability density function $f(\mathbf{z})$. This function indicates the relative plausibility of the possible values of the random variables $\mathbf{z} \in \Omega_z \subset R^{n_T}$. In what follows it is assumed without much loss of generality that the components of $\mathbf{z}$ are independent, that is, $f(\mathbf{z}) = \Pi_{j=1}^{N_T} f_j(z_j)$ where for every $j, f_j$ is a one-dimensional probability density function for $z_j$. It is noted that this is the case, for example, of stochastic excitations modeled in terms of Gaussian processes. This type of processes are important since allows to describe a wide range of cases such as filtered white noise processes, colored excitations, non-stationary excitations, etc. [36]. On the other hand, to estimate the robust failure probability that takes into account that the system model parameters are uncertain, a weighted integral of conditional failure probabilities over the whole parameter space must be evaluated. The weighting function in the integral is the probability density function of the possible models of the system. In the case where no dynamic data is available, the initial or prior probability density function $p(\boldsymbol{\theta}|M)$ of the model parameters is involved. Thus the robust failure probability can be written as

$$P(F|M) = \int_{\Theta} P(F|M,\boldsymbol{\theta}) p(\boldsymbol{\theta}|M) d\boldsymbol{\theta} \tag{13}$$

The dependence of the robust failure probability on the model class $M$ is clear from the above definition. This integral is difficult to evaluate unless only a small number of model parameters $\boldsymbol{\theta}$ are involved, so that numerical integration can be performed. Alternatively, Eq. (13) can be re-written in terms of the indicator function by using the characterization of the conditional failure probability in Eq. (12) as

$$P(F|M) = \int_{\Theta} \int_{\Omega_z} \Pi_F(\mathbf{z},\boldsymbol{\theta}|M)\, f(\mathbf{z})\, p(\boldsymbol{\theta}|M) d\mathbf{z} d\boldsymbol{\theta}. \tag{14}$$

The probability integrals in Eqs. (12) and (14), which have the same structure, usually involve a large number of random variables (hundreds or thousands) in the context of dynamical systems under stochastic excitation. Therefore, these integrals represent high-dimensional reliability problems. On the other hand, the normalized demand function that characterizes the failure domain $\Omega_F$ is usually not known explicitly in terms of the random variables, but must be computed point wise by applying suitable deterministic numerical techniques such as finite element analysis. The previous difficulties for estimating the nominal and robust failure probabilities favor the application of advanced Monte Carlo strategies as fundamental approaches to cope with the probability integrals [37–39]. In particular a generally applicable method, called subset simulation, is implemented in the present formulation [40,41].

#### 3.2.1. Reliability estimation

In the context of subset simulation, the failure probabilities are expressed as a product of conditional probabilities of some chosen intermediate failure domains, the evaluation of which only requires simulation of more frequent events. For example, the robust failure probability $P(F|M)$ is expressed as the product

$$P(F|M) = P[F_1(M)] \prod_{k=1}^{m_F-1} P[F_{k+1}(M)|F_k(M)], \tag{15}$$

where $F_{m_F}(M) = F(M)$ is the target failure domain, and $F_{m_F}(M) \subset F_{m_F-1}(M) \ldots \subset F_1(M)$ is a nested sequence of failure domains. It is seen that, even if $P(F|M)$ is small, by choosing $m_F$ and $F_k(M), k = 1, \ldots, m_F - 1$ appropriately, the conditional probabilities can still be made sufficiently large, and therefore they can be evaluated efficiently by simulation because the failure events are more frequent. Conditional failure probabilities equal to 0.1 are considered in the present formulation. Details of this simulation procedure from the theoretical and numerical viewpoint can be found in [40].

### 3.3. Updated robust failure probability

The updated robust failure probability is evaluated as an integral of the conditional failure probabilities weighted by the posterior probability density function $p(\boldsymbol{\theta}|M,D)$, that is,

$$P(F|M,D) = \int_{\Theta} P(F|M,\boldsymbol{\theta}) p(\boldsymbol{\theta}|M,D) d\boldsymbol{\theta}. \tag{16}$$

This integral, which is similar to the probability integral corresponding to the robust failure probability in Eq. (13), takes into account the information from the data through the use of the posterior probability density function of the model parameters. The integral is difficult to evaluate unless only a small number of model parameters $\boldsymbol{\theta}$ are involved, as previously

pointed out. Otherwise, more computational efficient approximations must be used. For example, when the posterior distribution $p(\boldsymbol{\theta}|M,D)$ is negligible except on a low-dimensional manifold in the parameter space $\boldsymbol{\theta}$ efficient asymptotic approximations have been proposed [10,21]. In those cases the Eq. (16) is estimated as a weighted sum of conditional probabilities of failure corresponding to a set of points on the manifold. This requires the characterization of the low-dimensional manifold by a discrete set of points non-uniformly distributed along the manifold. Note that for identifiable cases the manifold consists of isolated points which correspond to the optimal value of the model parameters. Although the approach based on asymptotic approximations has proved to be quite effective in a number of applications, it has certain limitations related to accuracy, especially when the problem is unidentifiable, or to computational inefficiency in searching for more than one global optimal point in the parameter space. Thus, a more general approach is considered here.

It is noted that substituting the expression of $P(F|M,\boldsymbol{\theta})$ from Eq. (12) into the integral, the updated robust failure probability can be re-written as a multidimensional integral over the space of the augmented parameter space of loading and system parameters as follows

$$P(F|M,D) = \int_{\Theta}\int_{\Omega_z} \Pi_F(\mathbf{z},\boldsymbol{\theta}|M)\, f(\mathbf{z})\, p(\boldsymbol{\theta}|M,D)\, d\mathbf{z}\, d\boldsymbol{\theta}. \tag{17}$$

This integral has the same form of the probability integral in Eq. (14), where the uncertain parameters involved in the problem are given by the vectors $\boldsymbol{\theta}$ and $\mathbf{z}$. However, the updated probability density function $p(\boldsymbol{\theta}|M,D)$ is not known explicitly. One alternative is to approximate the probability density of the parameters, for example, by means of multidimensional Gaussian kernels and then use simulation techniques such as direct subset simulation. Another option, which is considered in this work, is to apply a methodology that uses directly the set of samples generated at the last stage of the transitional Markov chain Monte Carlo method.

## 4. Updated robust reliability estimation

### 4.1. Direct approach

Using the set of samples generated at the last stage of the transitional Markov chain Monte Carlo method, $\boldsymbol{\theta}_m^l, l = 1,\ldots,N_m$, the updated robust failure probability can be estimated directly as

$$P(F|M,D) = \int_{\Theta} P(F|M,\boldsymbol{\theta}) p(\boldsymbol{\theta}|M,D) d\boldsymbol{\theta} = E(P(F|M,\boldsymbol{\theta})) \approx \frac{1}{N_m}\sum_{l=1}^{N_m} P(F|M,\boldsymbol{\theta}_m^l), \tag{18}$$

according to the law of large number. Note that this estimate is an asymptotically unbiased estimator of $E(P(F|M,\boldsymbol{\theta}))$ when the number of samples is large, because $\{\boldsymbol{\theta}_m^l, l = 1,\ldots,N_m\}$ are asymptotically distributed as $p(\boldsymbol{\theta}|M,D)$. While the previous estimation of the updated failure probability is direct, it may be quite involved from the numerical viewpoint in some cases. For example, for unidentifiable cases the estimation of a large number of conditional failure probabilities may be required. To cope with this difficulty an alternative implementation based on subset simulation is proposed in the following section.

### 4.2. Proposed strategy

#### 4.2.1. Unconditional samples

As previously pointed out the basic idea of subset simulation is to express the failure probability $P(F|M,D)$ as a product of a series of conditional probabilities. The updated robust failure probability is expressed as

$$P(F|M,D) = P[F_1(M,D)] \prod_{k=1}^{m_F-1} P[F_{k+1}(M,D)|F_k(M,D)], \tag{19}$$

where $F_{m_F}(M,D) \subset F_{m_F-1}(M,D) \ldots \subset F_1(M,D)$ is a nested sequence of failure domains. Note that the updated failure domains $(F_k(M,D), k = 1,\ldots,m_F)$ differ from the failure domains prior to data $(F_k(M), k = 1,\ldots,m_F)$. The probability of the first failure event, associated with the failure domain $F_1$, can be readily estimated by Monte Carlo simulation as

$$P[F_1(M,D)] \approx \frac{1}{N}\sum_{l=1}^{N} \Pi_{F_1}(\mathbf{q}^{l(0)}|M), \tag{20}$$

where $\mathbf{q}^{l(0)^T} = <\mathbf{z}^{l(0)^T}, \boldsymbol{\theta}^{l(0)^T}>$ denotes the samples corresponding to conditional level 0 (unconditional) of the augmented vector of uncertain parameters for the excitation $\mathbf{z}$ and the model parameters $\boldsymbol{\theta}$. The quantities $\mathbf{z}^{l(0)}, l = 1,\ldots,N$ are independent and identically distributed samples simulated according to the probability density function $f(\cdot)$. On the other hand, the samples $\boldsymbol{\theta}^{l(0)}, l = 1,\ldots,N$ are drawn from the set of samples generated at the last stage of the transitional Markov chain Monte Carlo method with probability

$$\bar{w}(\boldsymbol{\theta}^l) = \frac{w(\boldsymbol{\theta}^l)}{\sum_{k=1}^{N_m} w(\boldsymbol{\theta}^k)}, \tag{21}$$

where the plausibility weight of the sample $\boldsymbol{\theta}^k$ is given by $w(\boldsymbol{\theta}^k) = p(\boldsymbol{\theta}^k|M)\, p(D|M,\boldsymbol{\theta}^k), k = 1,\ldots,N_m$. This sample generation scheme can be interpreted as an acceptance-rejection algorithm where the proposal density function $\pi(\cdot)$ is defined as a discrete distribution over the samples generated at the last stage of the transitional Markov chain Monte Carlo method. The value of the distribution function at the sample $\boldsymbol{\theta}^k$ is just the normalized weight of that sample, that is, $\pi(\boldsymbol{\theta}^k) = \bar{w}(\boldsymbol{\theta}^k)$.

#### 4.2.2. Conditional samples

In order to estimate the conditional probabilities, a set of conditional samples are required. Following the idea of subset simulation, there will be a number of samples among $\mathbf{q}^{l(0)}, l = 1,\ldots,N$ lying in the failure domain $F_1$. Recall that the intermediate failure domains are chosen adaptively using information from simulated samples so that they correspond to some specific values of conditional failure probabilities. Starting from each of these conditional samples that lie in $F_1$, Markov chain Monte Carlo simulation is used to generate an additional number of conditional samples making up a total of $N$ conditional samples $\mathbf{q}^{l(1)}, l = 1,\ldots,N$ at conditional level 1. The conditional samples $\mathbf{q}^{l(1)}, l = 1,\ldots,N$ are used to estimate the conditional probability $P[F_2|F_1]$ as

$$P[F_2(M,D)|F_1(M,D)] \approx \frac{1}{N}\sum_{l=1}^{N}\Pi_{F_2}(\mathbf{q}^{l(1)}|M). \tag{22}$$

Again, there will be a number of samples among $\mathbf{q}^{l(1)}, l = 1,\ldots,N$ lying in the failure domain $F_2$. These samples provide the seeds for simulating an additional number of conditional samples making up a total of $N$ conditional samples $\mathbf{q}^{l(2)}, l = 1,\ldots,N$ at conditional level 2. Repeating this process, it is possible to generate conditional samples of higher conditional levels until the target failure probability has been reached.

#### 4.2.3. Markov chain samples

The idea is to generate a sequence of samples $\{\mathbf{q}^1, \mathbf{q}^2, \ldots\}$ from a given sample $\mathbf{q}^1$ by computing $\mathbf{q}^{k+1}$ from $\mathbf{q}^k$ $(k = 1,2,\ldots)$. In the context of this formulation it is assumed that the number of uncertain model parameters $\boldsymbol{\theta}$ is small compared with the number of random variables $\mathbf{z}$ that characterizes the stochastic excitation. In other words, the high-dimensionality of the reliability problem is due to the representation of the excitation. It is noted that this is the usual case encountered in stochastic dynamical systems. Based on the previous assumptions and the fact that the original Metropolis algorithm does not work in high-dimensional conditional probability spaces [19,20,40], the modified Metropolis algorithm [40] is used for generating the candidate states of the $\mathbf{z}$ vector, while the original algorithm is implemented for generating the candidate states of the $\boldsymbol{\theta}$ vector. Thus, for each component $z_j^k, j = 1,\ldots,N_T$ of the vector $\mathbf{z}^k$ (the first $N_T$ components of $\mathbf{q}^{k^T} =< \mathbf{z}^{k^T}, \boldsymbol{\theta}^{k^T} >$) a random number $\xi_j$ is simulated from a proposal probability density function $\pi_z(\cdot)$. In the present implementation a uniform probability density function centered at $z_j^k$ is selected. It is well known that the spread of the proposal probability density function affects the size of the region covered by the Markov chain samples. The optimal choice of the spread is a trade-off between acceptance rate and correlation. It has been shown that a good candidate for the spread of the distribution is such that the average acceptance rate of the proposed moves is roughly between 25% and 50% [42,43]. Of course, the optimal choice of the spread depends on the particular type of problem. Next, the ratio $r_j = f_j(\xi_j)/f_j(z_j^k)$ is computed. The auxiliary variable $\hat{z}_j^k$ is set as $\hat{z}_j^k = \xi_j$ with probability $\min(1, r_j)$ and $\hat{z}_j^k = z_j^k$ with probability $1 - \min(1, r_j)$. For the model parameters $\boldsymbol{\theta}$ a random vector $\boldsymbol{\varsigma}$ is simulated from a proposal probability density function $\pi_\theta(\cdot)$. This function is selected as a $n_p$-dimensional Gaussian distribution centered at the sample $\boldsymbol{\theta}^k$ with covariance matrix $\boldsymbol{\Sigma}_\theta$ given by

$$\boldsymbol{\Sigma}_\theta = \kappa^2 \sum_{l=1}^{N_m} \bar{w}(\boldsymbol{\theta}^l)[(\boldsymbol{\theta}^l - \bar{\boldsymbol{\theta}})(\boldsymbol{\theta}^l - \bar{\boldsymbol{\theta}})^T], \tag{23}$$

with

$$\bar{\boldsymbol{\theta}} = \sum_{l=1}^{N_m} \bar{w}(\boldsymbol{\theta}^l)\boldsymbol{\theta}^l, \quad \bar{w}(\boldsymbol{\theta}^l) = \frac{w(\boldsymbol{\theta}^l)}{\sum_{k=1}^{N_m} w(\boldsymbol{\theta}^k)}, \tag{24}$$

where $\kappa^2$ is a scaling parameter, and $\boldsymbol{\theta}^l, l = 1,\ldots,N_m$ is the set of samples generated at the last stage of the transitional Markov chain Monte Carlo method. Note that this proposal probability density function is similar to the one used in the identification process (see Section 2.5). Once the random vector $\boldsymbol{\varsigma}$ has been simulated the ratio $r = p(\boldsymbol{\varsigma}|M)\, p(D|M,\boldsymbol{\varsigma})|p(\boldsymbol{\theta}^k|M)\, P(D|M,\boldsymbol{\theta}^k)$ is computed. The auxiliary vector $\hat{\boldsymbol{\theta}}^k$ is set as $\hat{\boldsymbol{\theta}}^k = \boldsymbol{\varsigma}$ with probability $\min(1, r)$ and $\hat{\boldsymbol{\theta}}^k = \boldsymbol{\theta}^k$ with probability $1 - \min(1, r)$. The location of $\hat{\mathbf{q}}^{k^T} =< \hat{\mathbf{z}}^{k^T}, \hat{\boldsymbol{\theta}}^{k^T} >$ is finally checked. If $\hat{\mathbf{q}}^k \in F_i$, where $F_i$ is the corresponding intermediate failure domain, the sample is accepted as the next sample in the Markov chain, that is, $\mathbf{q}^{k+1} = \hat{\mathbf{q}}^k$. Otherwise the sample is rejected and the current sample is taken as the next sample, i.e., $\mathbf{q}^{k+1} = \mathbf{q}^k$.

Finally, it is noted that even though the conditional samples generated by Markov chain Monte Carlo simulation are dependent, the samples usually spread in the important regions of the uncertain parameter space. This is because the samples generated in the first stage of the updating procedure are obtained from direct Monte Carlo simulation for the $\mathbf{z}$ vector and from the last stage of the transitional Markov chain Monte Carlo method for the $\boldsymbol{\theta}$ vector. In addition, new Markov chain samples are generated at the tail of each chain during the entire procedure. Consequently, as long as the number of samples

is sufficiently large, the samples in the last stage are expected to also spread in the important regions of the uncertain parameter space. The number of samples used at each conditional level is equal to $N = 1000$ in the present implementation.

## 5. Applications

Three application problems are considered in this Section. The objective of the first application is to compare the reliability of a system at the initial design stage before any data are collected with the updated robust reliability at the operation stage during which the test data are collected. In the second application the effect of updated information about the system parameters on the behavior of a passive control design strategy is examined. Finally, the third application deals with the reliability of a base-isolated structural system in which changes in the behavior of the isolation system have occurred.

### 5.1. Application no. 1: updating reliability

#### 5.1.1. Description

Consider the two-story shear frame structure under earthquake loading shown in Fig. 1. The floor masses are $m_1 = m_2 = 1$, and the interstory stiffnesses are $k_1 = k_2 = 1000$. The actual damping ratios for the two vibrational modes are identical and equal to $\zeta = \zeta_1 = \zeta_2 = 0.03$. In what follows, it is assumed that this model is representative of the actual behavior of the frame structure and is referred to as the actual structure. In order to simulate modeling errors a model class $M$ (a 2DOF two-story linear shear building model class) is introduced. The interstory stiffnesses are parameterized as $k_1 = \theta_1 \bar{k}_1$ and $k_2 = \theta_2 \bar{k}_2$, where $\theta_1$ and $\theta_2$ are the stiffness parameters to be identified, and $\bar{k}_1 = \bar{k}_2 = 1450$ are references values for the interstory stiffness of the first and second floor, respectively. The masses for each model in $M$ is set equal to the actual system. The nominal model of the structure, which for a real structure would correspond to a pre-test model used in the design stage is taken from the class $M$ by specifying the values of the model parameters. In this case $\theta_1 = \theta_2 = 1.0$. Note that the nominal model is stiffer than the actual system. This is reasonable since the behavior of the actual structure is expected to be more flexible after deterioration from environmental effects has occurred. The structural model is excited horizontally by a ground acceleration $a(t)$. The ground acceleration is modeled as a non-stationary filtered white noise process and it is expressed as

$$a(t) = \Omega_1^2 w_1(t) + 2\xi_1\Omega_1 \frac{d}{dt}(w_1(t)) - \Omega_2^2 w_2(t) - 2\xi_2\Omega_2 \frac{d}{dt}(w_2(t)), \tag{25}$$

where the auxiliary functions $w_1(t)$ and $w_2(t)$ satisfy the second-order differential equations

$$\frac{d^2}{dt^2}(w_1(t)) + 2\xi_1\Omega_1 \frac{d}{dt}(w_1(t)) + \Omega_1^2 w_1(t) = \omega(t)\,\tau(t), \tag{26}$$

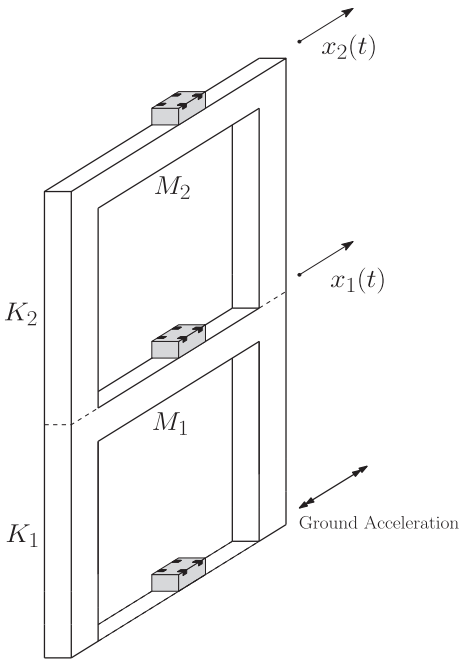


**Fig. 1.** Structural model under ground acceleration (base, first floor and second floor acceleration measurements).

$$\frac{d^2}{dt^2}(w_2(t)) + 2\xi_2\Omega_2\frac{d}{dt}(w_2(t)) + \Omega_2^2 w_2(t) = \Omega_1^2 w_1(t) + 2\xi_1\Omega_1\frac{d}{dt}(w_1(t)), \tag{27}$$

where $\omega(t)$ denotes white noise, and

$$\tau(t) = \frac{e^{-0.5t} - e^{-t}}{\max_t(e^{-0.5t} - e^{-t})}, \quad 0 < t < 10\ \text{s} \tag{28}$$

is the envelope function. The values $\Omega_1 = 15.0$ rad/s, $\xi_1 = 0.6, \Omega_2 = 1.0$ rad/s, and $\xi_2 = 0.9$, and white noise intensity $I = 3.5 \times 10^{-2}$ m$^2$/s$^3$ are used in the present application. This model corresponds in frequency content to the so-called Clough and Penzien filter [44]. The sampling interval and the duration of the excitation are taken as $\Delta t = 0.01$ s, and $T = 10$ s, respectively. Then, the discrete-time white noise sequence $\omega(t_j) = \sqrt{I/\Delta t}\, z_j$, where $z_j, j = 1, \ldots, 1001$, are independent, identically distributed standard Gaussian random variables is considered in this case.

*5.1.2. Identification process*

In what follows it is assumed that the structure is already built and response data are available. Thus, the model of the structure can be updated. The model updating is based on measurements of the ground acceleration $a(t)$ at the base and the absolute acceleration at the first and second floor of the structure. Simulated measured data are used in this example problem. To this end, the input ground acceleration time history is given in terms of the N–S component of the 2010 Chilean earthquake, Concepcion record (shown in Fig. 2). The actual input used for the identification process is the previous record scaled by a factor equal to 0.25. The measured response is simulated by first calculating the absolute acceleration response of the actual structure at the first and second floor and then adding 10% *rms* Gaussian white noise.

The prior probability density functions for the model parameters are independent uniform distributions defined over the interval $[0.0, 1.5]$. For identification purposes, the transitional Markov chain Monte Carlo method with $N_j = 1000,\ j = 1, \ldots, m$ is implemented (i.e., 1000 samples per stage). The scaling parameters ($\beta$ and $\kappa$) involved in Eqs. (8) and (23) are assumed to be equal 0.04. The samples, in terms of the stiffness parameters, obtained by the transitional Markov chain Monte Carlo method for some selected durations of the input ground acceleration are plotted in Fig. 3. Three cases are considered in the figure. Cases I, II, and III correspond to the identification process using 10 s, 20 s and 30 s of data, respectively. A sampling interval $\Delta t = 0.01$ s is used in all cases. It is seen that if the accelerations are measured for a short period of time (cases I and II), the posterior probability density function of the model parameters is relatively flat along certain directions in the parameter space (unidentifiable case). As the duration of the measured data increases to 30 s, the posterior probability density function concentrates in the vicinity of a peak located at $(0.69, 0.69)$ (global identifiable case). The corresponding histograms of the interstory stiffnesses defined by the posterior samples are shown in Figs. 4–6 for cases I, II and III, respectively. In addition, the values of the properties of the nominal system are also shown in the figures. The spread of the samples for cases I and II (unidentifiable cases) is clear from the histograms. On the other hand it is observed that the agreement between the actual system ($k_1 = k_2 = 1000$) and the model characterized by the posterior samples is very good for the case III (global identifiable case). Hence, the data used in the identification procedure provides enough information in order to shift the nominal properties to the target values and to reduce the initial uncertainty in this case. It is noted that for the global identifiable case the optimal model parameters can be obtained directly by finding the minimum of the measure-of-fit function given by Eq. (4).

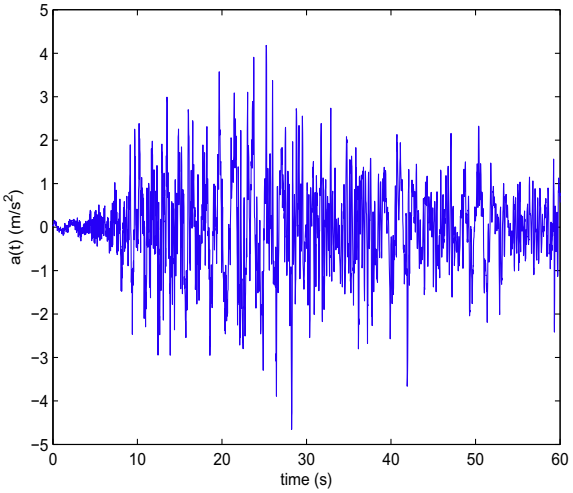


**Fig. 2.** N–S component of the 2010 Chilean earthquake, Concepcion record.

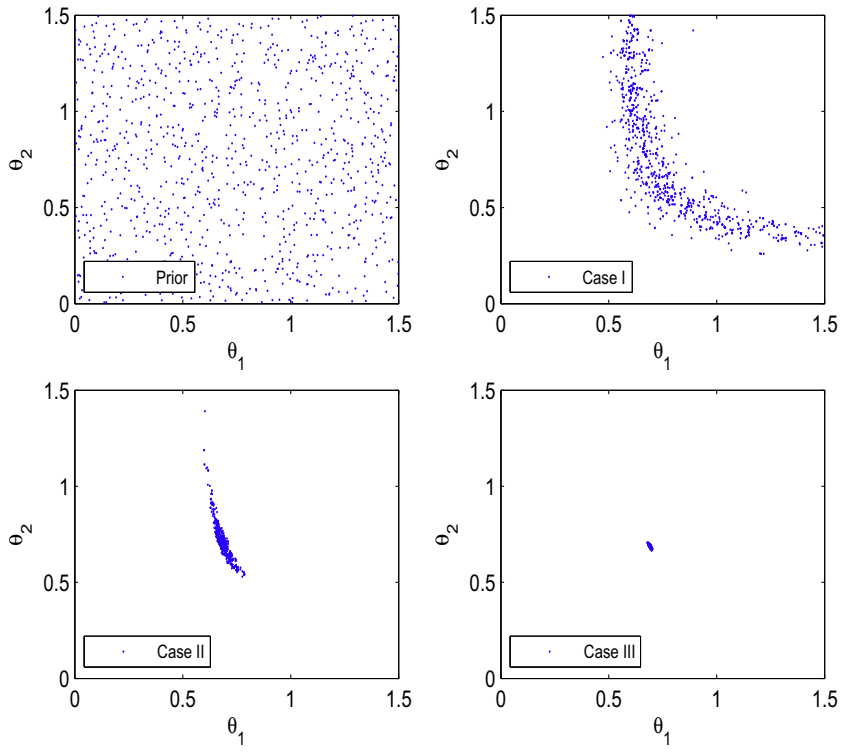


**Fig. 3.** Samples of the stiffness parameters obtained by the transitional Markov chain Monte Carlo method for selected durations of the input ground acceleration. Case I: accelerations measured for 10 s. Case II: accelerations measured for 20 s. Case III: accelerations measured for 30 s.

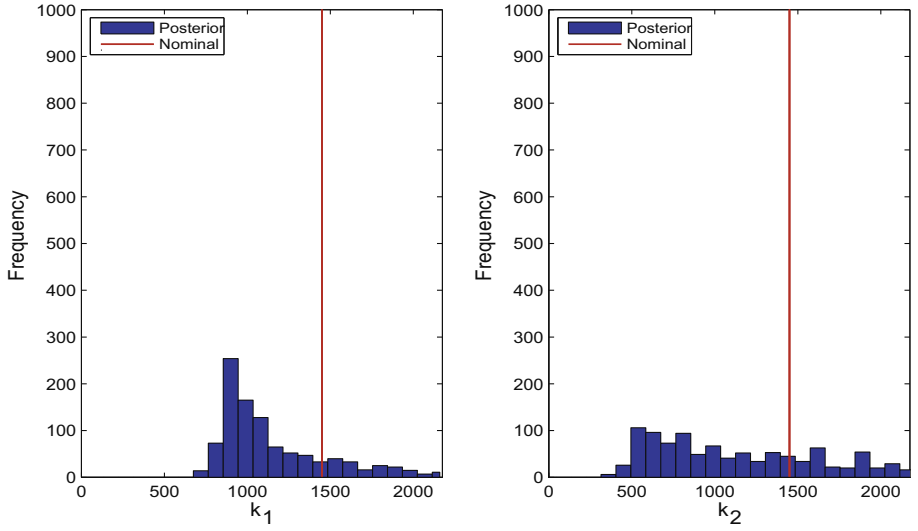


**Fig. 4.** Posterior histogram of the interstory stiffnesses for the unidentifiable case (Case I).

### 5.1.3. Failure probability

The system is considered to have failed under earthquake excitation if some stochastic dynamic responses exceed within a specified time interval $[0, T]$ certain critical upper bounds. In particular the following failure domain $F$ is considered

$$F(M) = \left\{ \mathbf{q}^T = < \mathbf{z}^T, \boldsymbol{\theta}^T > | d(\mathbf{q}|M) = \max_{j=1,2} \max_{t \in [0,T]} \frac{|r_j(t, \mathbf{z}, \boldsymbol{\theta})|}{r^*} > 1 \right\}, \tag{29}$$

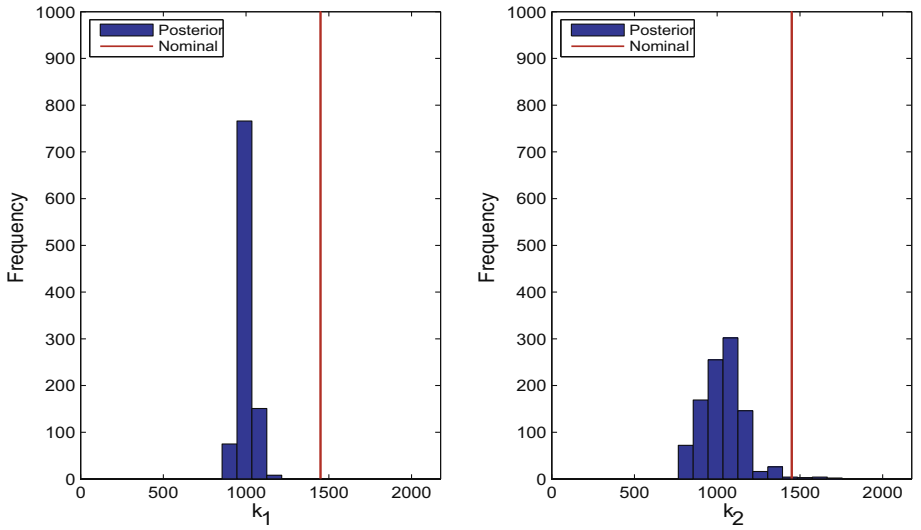


**Fig. 5.** Posterior histogram of the interstory stiffnesses for the unidentifiable case (Case II).

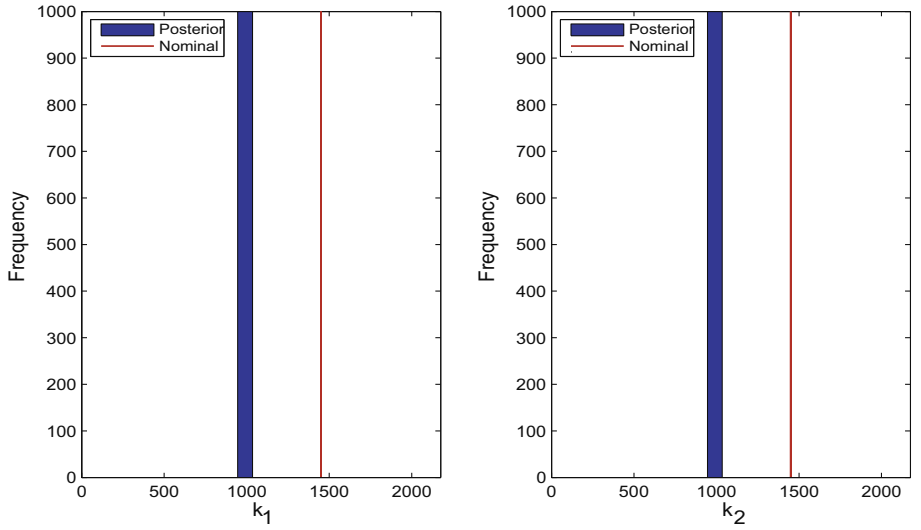


**Fig. 6.** Posterior histogram of the interstory stiffnesses for the identifiable case (Case III).

where $\mathbf{q}$ is the augmented vector of system parameters, $r_j(t, \mathbf{z}, \boldsymbol{\theta})$ is the relative displacement between the $(j-1, j)$th floors, $r^*$ is the critical threshold level and all other terms have been previously defined. The response functions $r_j(\cdot, \cdot, \cdot), j = 1, 2$ are obtained from the solution of the equation of motion that characterizes the model class $M$. The threshold level $r^*$ is calibrated such that the probability of failure of the nominal system is equal to $10^{-4}$. Note that the estimation of the failure probabilities represents a high-dimensional reliability problem in this case. In fact more than a thousand random variables are involved in the corresponding multidimensional probability integrals. Table 1 shows the failure probability of the updated and actual system using an average of 50 independent runs. For the unidentifiable cases the failure probabilities are computed by the proposed strategy. On the other hand, the probability of failure for the identifiable case is just the failure probability function evaluated at the most probable value of the model parameters.

It is observed that the updated robust failure probability and the actual failure probability are very similar when the duration of the data is relatively large (30 s). This result is expected since this case corresponds to the global identifiable case. For the unidentifiable cases the robust failure probabilities are higher than the actual system due to the uncertainty of the model class parameters (stiffness parameters). In other words, the parametric uncertainties increase the probability of failure in relation to the probability of failure obtained from the global identifiable case, which has associated very small parameter uncertainties. For example it is seen that for Cases I and II there are a number of samples that make the system more flexible

**Table 1**
Failure probability of the updated and actual system for some selected duration of the identification process.

| Cases | Failure probability | |
|---|---|---|
| | Updated system | Actual system |
| I: Unidentifiable case | $7.5 \times 10^{-2}$ | $3.9 \times 10^{-2}$ |
| II: Unidentifiable case | $4.4 \times 10^{-2}$ | $3.9 \times 10^{-2}$ |
| III: Identifiable case | $3.9 \times 10^{-2}$ | $3.9 \times 10^{-2}$ |

in the first floor ($\theta_1 < 0.69$), increasing in this manner the failure probability (see Fig. 3). Table 2 shows the corresponding failure probabilities estimated directly by the samples generated al the last stage of the transitional Markov chain Monte Carlo method (Eq. 18) for Cases I and II. The estimates are of the same order to the ones obtained by the proposed scheme. However, the computational cost (CPU time) involved in the evaluation of the estimator $E(P(F|M,\boldsymbol{\theta}))$ is about two order of magnitude greater than the corresponding cost of the proposed implementation.

To investigate the variability of the estimates, the sample COV (coefficient of variation) of the updated failure probability is computed from 50 independent runs. This information is provided in Table 3, where it is seen that the variability of the estimates is relatively small for all cases.

It turns out that the rejection rate for the model class parameters during the identification process is quite high (above 80%) for the unidentifiable cases. Under this condition the generation of new samples for the model parameters at the conditional levels may be avoided. Table 4 shows the impact of rejecting the samples for the model parameters at the conditional levels on the failure probability estimates. The third column of the table corresponds to the case where the samples generated by the proposal probability density function are always rejected (acceptance option not activated in Table 4). In this case the same samples $\boldsymbol{\theta}$ drawn at the first level (unconditional level) are used during the higher levels. It is seen that the estimates are almost identical. Therefore, the generation of new samples from the proposal probability density function can be avoided in this case. This in turn increases the efficiency of the proposed implementation since the number of model responses (dynamic analyses) is reduced during the updating procedure. The samples generated by the two implementations (acceptance option activated/not-activated) at the last conditional level of the proposed strategy for one particular run are shown in Fig. 7. It is observed that the distribution of the selected samples in the model parameter space is very similar for both cases. Consequently, the probability of failure estimates are very similar as indicated before.

The numerical efforts associated with the identification process and the estimation of the updated failure probability (by means of the proposed method) are summarized in Table 5. The first column of this table indicates the type of analysis or process performed, while the next three columns show the number of model evaluations (dynamic analyses) required for cases I, II and III, respectively.

Finally, the effect of monitoring data on the system failure probability is investigated for the global identifiable case. Recall that this case has associated very small parameter uncertainties. In Table 6 the updated robust failure probability is compared with the failure probability of different nominal systems. The nominal systems are defined in terms of the value of the stiffness parameters $\theta_1$ and $\theta_2$. The selection of threshold level $r^*$, representing the demand in design, is such that the nominal failure probability is equal to $10^{-4}$. The choice $\theta_1 = \theta_2 = 1.0$ (first row of the table), which corresponds to case III reported in Table 1, can be interpreted as the case where significant changes in the stiffnesses of the nominal system have occurred. On the other hand, the case $\theta_1 = \theta_2 = 0.70$ (last row of the table) may correspond to small changes in the properties

**Table 2**
Failure probability of the updated system calculated directly by the samples generated al the last stage of the transitional Markov chain Monte Carlo method (Eq. 18).

| Cases | Failure probability |
|---|---|
| I: Unidentifiable case | $8.0 \times 10^{-2}$ |
| II: Unidentifiable case | $4.6 \times 10^{-2}$ |

**Table 3**
Variability of the updated failure probability estimates

| Cases | Failure probability | |
|---|---|---|
| | Estimate | Coefficient of variation |
| I: Unidentifiable case | $7.5 \times 10^{-2}$ | 0.11 |
| II: Unidentifiable case | $4.4 \times 10^{-2}$ | 0.11 |
| III: Identifiable case | $3.9 \times 10^{-2}$ | 0.11 |

**Table 4**
Probability of failure of the updated system for some selected duration of the identification process.

| Cases | Failure probability | |
|---|---|---|
| | Acceptance option activated | Acceptance option not-activated |
| I: Unidentifiable case | $7.5 \times 10^{-2}$ | $7.4 \times 10^{-2}$ |
| II: Unidentifiable case | $4.4 \times 10^{-2}$ | $4.3 \times 10^{-2}$ |

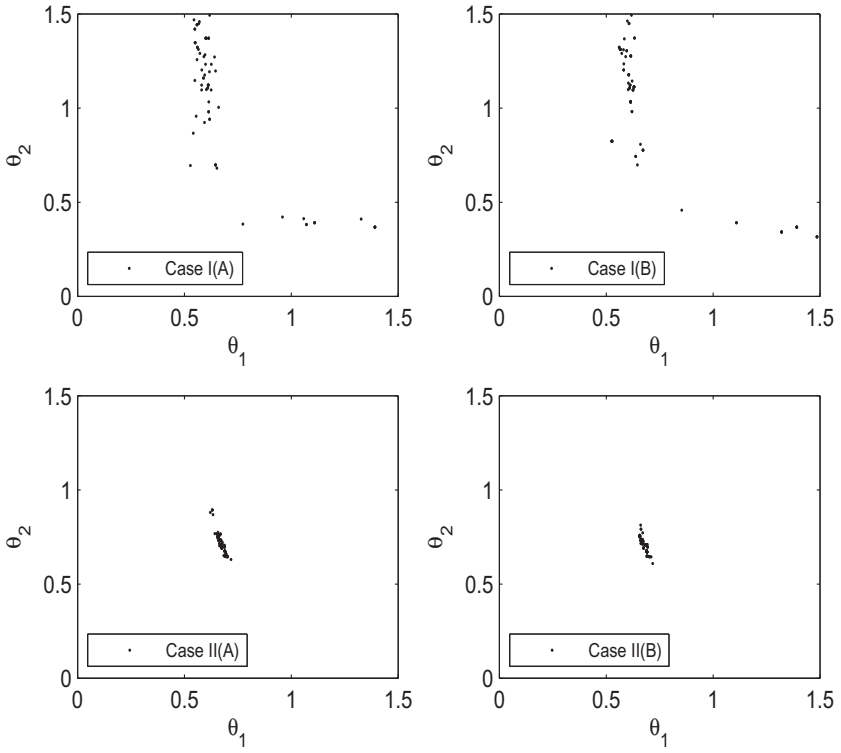


**Fig. 7.** Samples of the stiffness parameters at the last conditional level of the proposed strategy. Case I: accelerations measured for 10 s. Case II: accelerations measured for 20 s. (A) Acceptance option activated. (B) Acceptance option not-activated.

of the nominal system. Recall that the updated system is defined in terms of $\theta_1 = \theta_2 = 0.69$. The other cases represent intermediate levels of changes in the properties of the nominal system. Note that the updated probability changes from row to row because the threshold $r^*$ is changed to keep the nominal failure probability at a constant level. It is seen that the updated failure probability is significantly larger than the nominal failure probability for cases where the level of model error, defined in terms of the parameters $\theta_1$ and $\theta_2$, is significant. Therefore, it can be concluded that monitoring data is very important since the updated model can differ significantly from the nominal model. Consequently monitoring data makes a difference in the estimation of the system reliability.

### *5.2. Application no. 2: a control design strategy*

#### *5.2.1. Nominal system*

The objective of this example is to evaluate the effect of the additional information gained about the structure from measured data on the performance of a passive energy dissipation system. For this purpose, the two-story reinforced concrete structure under earthquake loading shown in Figs. 8 and 9 is considered. Forty-eight columns of square cross section support each floor. The dimension of the columns are equal to 0.57 m and 0.53 m for the first and second floor, respectively. Both floors have a constant height of 3.0 m. The mass of each floor is equal to 1260 ton. The behavior of the reinforced concrete structure is characterized by considering a Young's modulus equal to $E = 2.5 \times 10^{10}$ N/m$^2$ and Poisson ratio $\nu = 0.3$. This model may be interpreted as the structural model obtained during the design phase. The structure is excited horizontally by a ground acceleration applied at 45° with respect to the $x$ axis. The induced ground acceleration is modeled as described

**Table 5**
Summary of numerical efforts associated with the identification process and the estimation of the updated failure probability.

| Type of process | Number of model evaluations | | |
|---|---|---|---|
| | Case I | Case II | Case III |
| Identification | 4000 | 7000 | 7000 |
| Failure probability[a] | 3800 | 3800 | 3800 |
| Failure probability[b] | 2900 | 2900 | 2900 |

[a] Acceptance option activated.
[b] Acceptance option not-activated.

**Table 6**
Effect of monitoring data on the updated failure probability for different nominal systems. Case III (global identifiable case)

| Parameters | Failure probability | |
|---|---|---|
| | Nominal system | Updated system |
| $\theta_1 = 1.00,\ \theta_2 = 1.00$ | $1.0 \times 10^{-4}$ | $3.9 \times 10^{-2}$ |
| $\theta_1 = 0.95,\ \theta_2 = 0.95$ | $1.0 \times 10^{-4}$ | $2.3 \times 10^{-2}$ |
| $\theta_1 = 0.90,\ \theta_2 = 0.90$ | $1.0 \times 10^{-4}$ | $1.3 \times 10^{-2}$ |
| $\theta_1 = 0.85,\ \theta_2 = 0.85$ | $1.0 \times 10^{-4}$ | $8.6 \times 10^{-3}$ |
| $\theta_1 = 0.80,\ \theta_2 = 0.80$ | $1.0 \times 10^{-4}$ | $1.2 \times 10^{-3}$ |
| $\theta_1 = 0.75,\ \theta_2 = 0.75$ | $1.0 \times 10^{-4}$ | $5.8 \times 10^{-4}$ |
| $\theta_1 = 0.70,\ \theta_2 = 0.70$ | $1.0 \times 10^{-4}$ | $1.1 \times 10^{-4}$ |

in the following section. For an improved earthquake performance the structure is reinforced with friction hysteretic devices at each floor. The devices follow the restoring force law

$$r(t) = k_d\big(\delta(t) - \gamma^1(t) + \gamma^2(t)\big), \tag{30}$$

where $k_d$ denotes the stiffness of the device, $\delta(t)$ is the relative displacement between floors, and $\gamma^1(t)$ and $\gamma^2(t)$ denote the plastic elongations of the friction device. Using the supplementary variable $s(t) = \delta(t) - \gamma^1(t) + \gamma^2(t)$, the plastic elongations are specified by the nonlinear differential equations [45]

$$\dot{\gamma}^1(t) = \dot{\delta}(t)H(\dot{\delta}(t))\left[H(s(t) - s_y)\frac{s(t) - s_y}{s_p - s_y}H(s_p - s(t)) + H(s(t) - s_p)\right],$$

$$\dot{\gamma}^2(t) = -\dot{\delta}(t)H(-\dot{\delta}(t))\left[H(-s(t) - s_y)\frac{-s(t) - s_y}{s_p - s_y}H(s_p + s(t)) + H(-s(t) - s_p)\right], \tag{31}$$

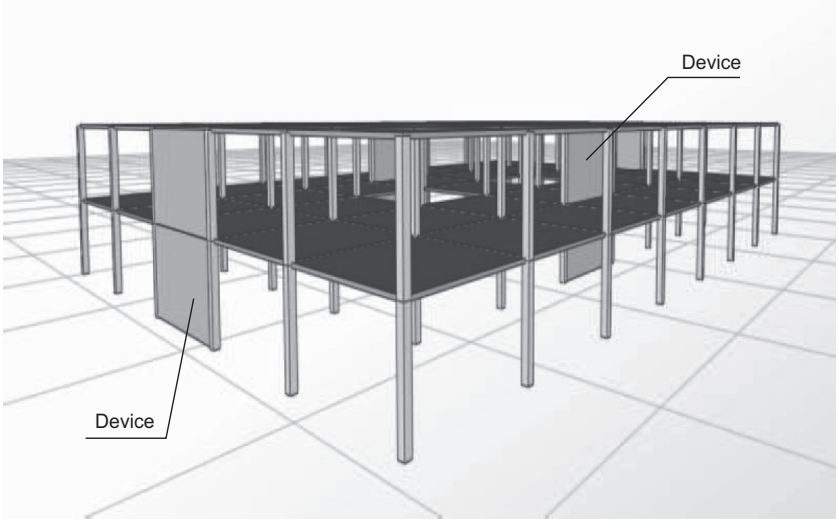


**Fig. 8.** Isometric view of the structural model.

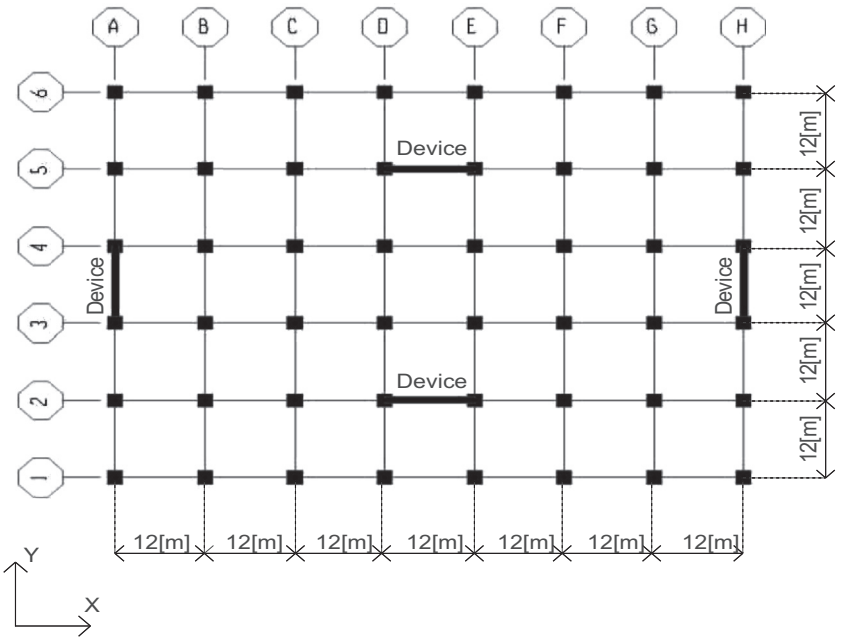


**Fig. 9.** Plan view of the structural model.

where $H(\cdot)$ denotes the Heaviside step function, $s_y$ is a parameter specifying the onset of yielding, and $k_d\, s_p$ is the maximum restoring force of the friction device. The values $s_p = 0.006$ m and $s_y = 0.0042$ m are used in this case. Because of the yielding, energy dissipation due to hysteresis is introduced in the structural response.

*5.2.2. Excitation model*

The ground acceleration is modeled as a non-stationary stochastic process. In particular, a point-source model characterized by the moment magnitude $M$ and epicentral distance $r$ is considered here [46,47]. The model is a simple, yet powerful means for simulating ground motions and it has been successfully applied in the context of earthquake engineering. The time-history of the ground acceleration for a given magnitude $M$ and epicentral distance $r$ is obtained by generating first a discrete-time white noise sequence $\omega(t_j) = \sqrt{2\pi/\Delta t}\, z_j, j = 1, \ldots, n_z$, where $z_j, j = 1, \ldots, n_z$, are independent, identically distributed standard Gaussian random variables, $\Delta t$ is the sampling interval, and $n_z$ is the number of time instants equal to the duration of the excitation $T$ divided by the sampling interval. The sampling interval and the duration of the excitation are taken equal to $\Delta t = 0.01$ (s) and $T = 20.0$ (s), respectively in this case. Then, the discrete-time Gaussian white noise sequence needed in the excitation model involves 2000 random variables. The white noise sequence is then modulated by an envelope function $h(t, M, r)$ at the discrete time instants. The modulated white noise sequence is transformed to the frequency domain by applying the discrete Fourier transform. The resulting spectrum is normalized by the square root of the average square amplitude spectrum. The normalized spectrum is then multiplied by a ground motion spectrum $S(f, M, r)$ at discrete frequencies $f_l = l/T, l = 1, \ldots, n_z/2$. Finally, discrete inverse Fourier transform is applied to transform the sequence back to the time domain to yield the desired ground acceleration time history. The particular values of the moment magnitude and epicentral distance used in this example are $M = 7$(dyn-cm) and $r = 15$ (km), respectively. For illustration purposes Fig. 10 shows a typical envelope function and ground motion spectrum and a corresponding sample of ground motion. Details of the characterization of the envelope function $h(t, M, r)$ and the ground acceleration spectrum $S(f, M, r)$ can be found in [46–49].

*5.2.3. Updated system*

For identification purposes, the following model class $M$ is considered. It is assumed that each floor may be represented as rigid within the $x$–$y$ plane when compared with the flexibility of the columns. Hence, each floor is represented by three degrees of freedom, i.e., two translatory displacements in the direction of the $x$ and $y$ axis, and a rotational displacement. Due to modeling errors the rigidities of the actual class of models are parameterized as: $EI_{1x} = \theta_1 E\bar{I}_{1x}, EI_{2x} = \theta_2 E\bar{I}_{2x}, EI_{1y} = \theta_3 E\bar{I}_{1y}$, and $EI_{2y} = \theta_4 E\bar{I}_{2y}$, where $\bar{I}_{ix}$ and $\bar{I}_{iy}, i = 1, 2$ represent the nominal moment of inertia of the columns of the $i$ floor in the $x$ and $y$ direction, respectively. These nominal values correspond to the columns of the nominal system previously described. On the other hand, the damping ratios for the vibrational modes are identical and parameterized as $\zeta = \theta_5 \bar{\zeta}$ where $\bar{\zeta}$ is the nominal value and equal to 3%. As in the previous example simulated measured data are used for the identification process. For illustration purposes the actual structure used to generate the measured data corresponds to a finite element model with about 5000 degrees of freedom, which includes beam, column and shell elements. The moment of inertia of the columns

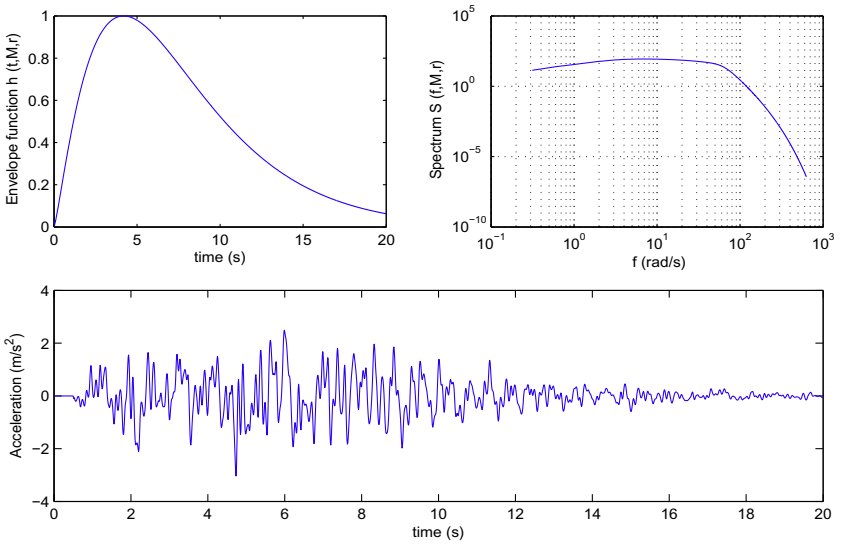


**Fig. 10.** Envelope function, ground motion spectrum, and a sample ground motion.

are defined in terms of the nominal properties as: $I_{1x} = 0.8\bar{I}_{1x}, I_{2x} = 0.9\bar{I}_{2x}, I_{1y} = 0.9\bar{I}_{1y}$, and $I_{2y} = 0.95\bar{I}_{2y}$. On the other hand, the actual damping ratios for the vibrational modes that contribute significantly to the response are identical and equal to $1.2\bar{\zeta}$. Note that the actual structure does not correspond to any model in the class of models considered. This actual structure may correspond to the structural system already built where changes in the stiffness and damping properties have occurred due to, for example, large response levels. The input ground acceleration history is taken as the one shown in Fig. 2 applied at 45° with respect to the $x$ axis. The measured response is simulated by first calculating the absolute acceleration response of the actual structure at the first and second floor (in the $x$ and $y$ direction) and then adding 15% *rms* Gaussian white noise. The responses are computed at the center of mass of each floor.

Thirty seconds of data with sampling interval $\Delta t = 0.01$ s were used, given a total of $N_t = 3000$ data points. Independent uniform prior distributions are assumed for the parameters $\theta_1, \theta_2, \theta_3, \theta_4$, and $\theta_5$ over the ranges $[0.5, 1.5]$ and $[0.9, 1.4]$ respectively. The transitional Markov chain Monte Carlo method with $N_j = 1000, j = 1, \ldots, m$ is implemented for the identification process. The scaling parameters $\beta$ and $\kappa$ are taken as 0.04 in this application problem. The four components of the samples corresponding to the rigidity parameters are shown in Fig. 11 in two groups: $\theta_1$ versus $\theta_2$ and $\theta_3$ versus $\theta_4$. The values of the parameters of the nominal system are also indicated in the figure.

The posterior samples are concentrated around the reference values $(0.8, 0.9)$ and $(0.9, 0.95)$, respectively, leading to a relatively peaked posterior probability density function. Recall that the reference values correspond to the model used to generate the measure data (actual structure). From Fig. 11 it is also observed that the data is strongly correlated along certain directions in the parameter space. Actually, there is a line of maximum likelihood estimates in the vicinity of the reference values in the $\theta_1 - \theta_2$ and $\theta_3 - \theta_4$ spaces. Note that the lines have negative slopes, which is reasonable since for example an increase in the stiffness of the first floor in the $x$ direction is compensated by a decrease in the stiffness of the second floor in the $x$ direction during the updating process. In other words, all points along that direction correspond to structural models that have almost the same response at the measured degrees of freedom. On the other hand, the histogram of the damping parameter shown in Fig. 12 indicates that the initial uncertainty about this parameter (interval $[0.9, 1.4]$) can be updated, which is deduced by the fact that the posterior samples are concentrated in a smaller range if compared with the prior samples. The updating procedure revels that the values in the range $[1.15, 1.35]$ with a concentration around 1.2 are more plausible based on the prior knowledge and on the data. The number of model evaluations required for performing the identification process is equal to 10000 in this case.

*5.2.4. System performance*

To evaluate the performance of the structural system the following failure domain is considered

$$F(M) = \left\{ \mathbf{q}^T =< \mathbf{z}^T, \boldsymbol{\theta}^T > | d(\mathbf{q}|M) = \max_{j=1,2} \max_{t\in[0,T]} \{ \frac{|r_{jx}(t,\mathbf{z},\boldsymbol{\theta})|}{r_x^*}, \frac{|r_{jy}(t,\mathbf{z},\boldsymbol{\theta})|}{r_y^*} \} > 1 \right\}, \tag{32}$$

where $\mathbf{q}$ represents the augmented vector of system parameters, $r_{jx}(t,\mathbf{z},\boldsymbol{\theta})$ and $r_{jy}(t,\mathbf{z},\boldsymbol{\theta})$ represent the relative displacement between the $(j-1,j)$th floor in the $x$ and $y$ direction, respectively, and $r_x^*$ and $r_y^*$ are the corresponding threshold levels. The critical response levels are calibrated such that the probability of failure of the reinforced nominal system is equal to $10^{-4}$. As in the previous application problem the estimation of the failure probabilities represents a high-dimensional reliability

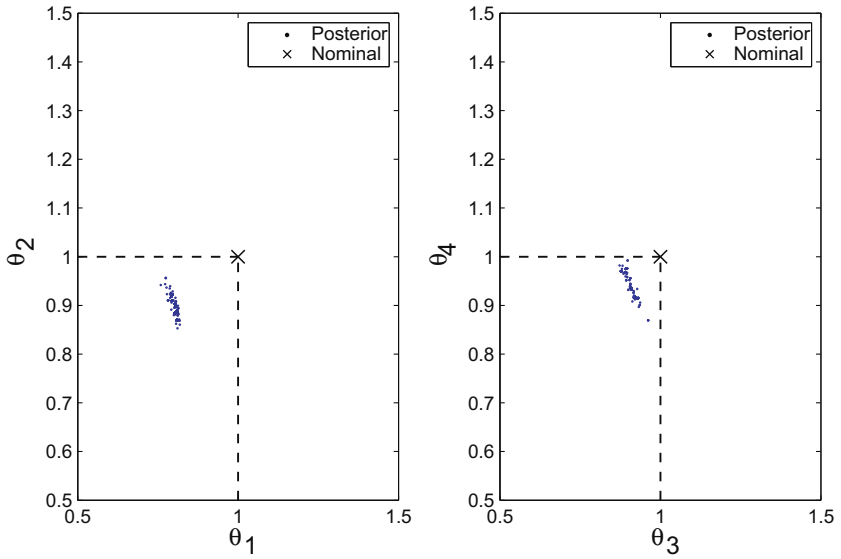


**Fig. 11.** Samples of the rigidity parameters obtained by the transitional Markov chain Monte Carlo method.

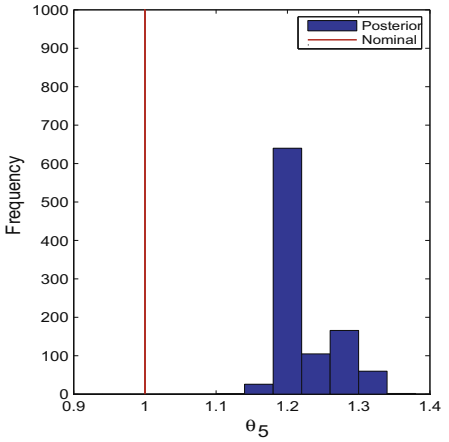


**Fig. 12.** Histogram of the damping parameter obtained by the transitional Markov chain Monte Carlo method.

problem (more than two thousand random variables are involved in the corresponding multidimensional probability integrals in this case). For calibration purposes the initial stiffness of the hysteretic devices is set equal to $k_d = 10 \times \bar{k}_d$, where $\bar{k}_d$ is a percentage of the stiffness of the first floor in the $x$ direction (1% in this case). Fig. 13 shows the failure probability of the nominal, updated most probable and updated models in terms of the initial stiffness of the nonlinear devices. The updated most probable model is defined in terms of the mean value of the parameters obtained at the last stage of the transitional Markov chain Monte Carlo method. Thus, this model does not involve parameter uncertainties. In addition, the curve obtained by taking into account prior uncertainties is also included in the figure. To be consistent with the Bayesian model updating considered before, independent uniform distributions are assumed for the prior distributions. Of course, other distributions can be considered as well. For example prior uncertainties can be quantified by Gaussian models with mean values equal to the nominal values of the model parameters and uncertainties assigned by user-specified covariance matrices. The updated robust probability of failure is computed by the proposed strategy while the probability of the other models are estimated by direct subset simulation. The same properties are assumed for the devices placed in the first and second floor. A range between 0 and $20 \times \bar{k}_d$ is considered in the figure. Note that zero initial stiffness corresponds to the linear model, i.e., the structural system without the hysteretic devices. It is observed that the probability of failure decreases as the initial stiffness of the nonlinear devices increases for all cases. This is reasonable since the structural model becomes stiffer when the initial stiffness increases and at the same time the devices introduce additional energy dissipation capacity to the structural system. In this regard, the use of friction hysteretic devices constitutes an effective control strategy.

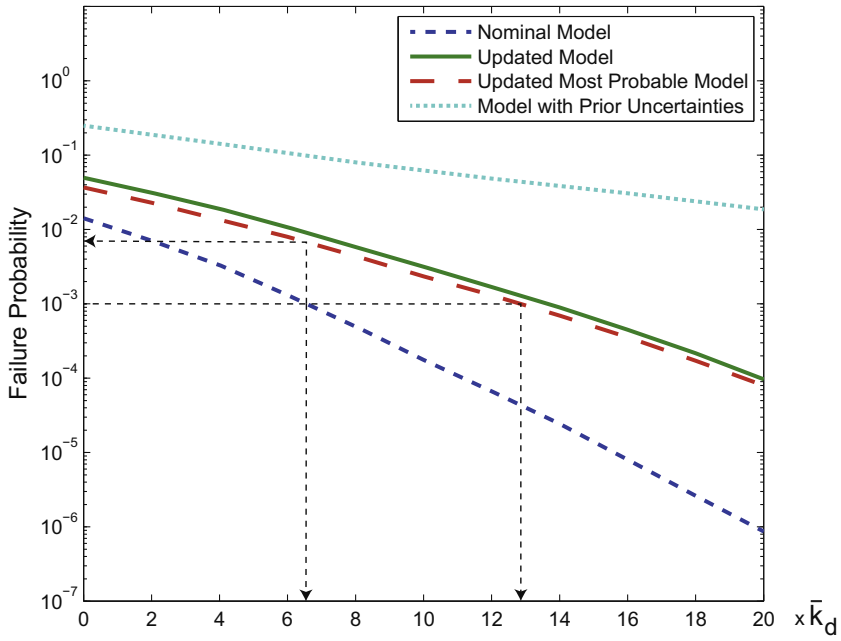


**Fig. 13.** Failure probability of the nominal model, updated most probable model, model with prior uncertainties and updated model in terms of the initial stiffness of the hysteretic devices.

Comparison of the curves obtained by the updated most probable model and the nominal system demonstrates the effect of monitoring data on the system failure probability. The failure probability of the updated most probable model is significantly larger than the corresponding to the nominal system. For example, if a probability of failure equal to $10^{-3}$ is imposed as a design requirement the initial stiffness of the devices required in the nominal system is approximately $7 \times \bar{k}_d$ while devices with initial stiffness equal to $13 \times \bar{k}_d$ are required for the updated most probable system. In other words, the updated most probable structural model reinforced with the devices used in the nominal system is not feasible under the prescribed reliability requirement since the failure probability would be close to $10^{-2}$ (see Fig. 13). Then, the reliability of the structural system computed before and after using dynamic data can differ significantly. It is noted that the numerical efforts involved in the estimation of the updated failure probability depend on the level of reliability. In fact the number of model evaluations is given in terms of the number of conditional levels required by the proposed strategy and the number of samples used at each level. The number of analyses involved in the estimation of the updated failure probabilities shown in Fig. 13 varies between 2000 and 7400, depending on the value of the failure probability.

*5.2.5. Effect of parameter uncertainty*

The effect of parameter uncertainty on the robust failure probability is illustrated by comparing the curves obtained by the updated model and the one that considers prior uncertainties. In general, the uncertainties tend to increase the robust probability of failure. In fact, it is observed from Fig. 13 that the values of the curve corresponding to the prior robust failure probability are larger than the ones for the updated robust failure probability. One of the reasons of this difference is the fact that the posterior samples (see Fig. 11) are concentrated in a smaller range if compared with the prior samples (uniformly distributed in the entire range). Consequently, the posterior robust failure probability decreases with respect to the prior robust failure probability. The difference is more than one order of magnitude for the range of initial stiffness of the nonlinear devices considered. Thus, the effect of the additional information gained about the structure from measured data on the performance of the structural system is considerable.

The effect of parameter uncertainty on the performance of the proposed control strategy can also be seen in Figs. 14 and 15. In these figures, the iso-probability curves corresponding to the system with prior uncertainties and the updated system in terms of the initial stiffnesses of the devices placed in the first and second floor are presented, respectively. Note that the devices placed in the first and second floor may have different properties in this case. The distribution of the iso-probability curves is quite different for these two systems. It is observed that the iso-probability curves corresponding to the updated system are essentially the curves of the system with prior uncertainties shifted towards the lower section of the stiffness parameters space. In fact, in order to obtain the same level of reliability, the stiffness of the devices placed in the system with prior uncertainties should be greater than the ones used in the updated system. For example, devices with initial stiffness close to $2 \times \bar{k}_d$ in both floors are associated with a probability of failure equal to $3.0 \times 10^{-2}$ for the updated system (point marked in Fig. 15). Contrarily, devices with initial stiffness close to $15 \times \bar{k}_d$ in both floors (point marked in Fig. 14) give

the same level of reliability for the system with prior uncertainties. Then, the effectiveness of the hysteretic devices changes dramatically due to the additional information gained about the system from measured data. Therefore, the resulting modeling uncertainties makes a difference in the performance evaluation of the passive energy dissipation system.

### 5.3. Application no. 3: base-isolation system performance

#### 5.3.1. Structural model

The three-dimensional reinforced concrete building model with a base isolation system shown in Fig. 16 is considered for analysis. Material properties of the reinforced concrete structure have been assumed as follows: Young's modulus $E = 2.5 \times 10^{10}$ N/m$^2$; and Poisson ratio $v = 0.2$. The total mass of the first and second floor is $7.0 \times 10^5$ kg, and $6.0 \times 10^5$ kg, respectively. On the other hand, the total mass of the platform is equal to $6.0 \times 10^5$ kg. The height of each floor is 3.5 m and the diaphragms are modeled with shell elements with a thickness of 0.25 m. Additionally, beam and column elements are used in the finite element model, which has a total of 7000 degrees of freedom. A 5% of critical damping is added to the first modes of the superstructure. For anti-seismic design purposes the superstructure is equipped with a total number of 20 rubber bearings in its isolation system. These devices consists of layers of rubber and steel, with the rubber being vulcanized to the steel plates. Fig. 17 shows a schematic representation of a rubber bearing, where $D_e$ represents the external diameter of the isolator, $D_i$ indicates the internal diameter, $H_r = t_r n_r$ is the total height of rubber in the device, $t_r$ is the layer thickness and $n_r$ is the number of rubber layers. The nominal values of the isolator parameters are set equal to $\bar{D}_e = 0.85$ m, $\bar{H}_r = 0.17$ m, and $\bar{D}_i = 0.10$ m. The force displacement characteristics of the isolator elements are modeled by a biaxial hysteretic behavior. An analytical model based on a series of experimental tests is used in the present application. A brief description of the model is provided in a subsequent section.

#### 5.3.2. Structural response

The structural system is excited by a ground acceleration in the $x$ direction. The excitation is modeled as in the previous application (see Application no. 2). The response of the base-isolated structural system is obtained from the solution of the equation of motion that characterizes the model. The equation of motion of the superstructure can be expressed in the form

$$\mathbf{M}_s\ddot{\mathbf{x}}_s(t) + \mathbf{C}_s\dot{\mathbf{x}}_s(t) + \mathbf{K}_s\mathbf{x}_s(t) = -\mathbf{M}_s\mathbf{G}_s(\ddot{\mathbf{x}}_b(t) + \ddot{\mathbf{x}}_g(t)), \tag{33}$$

where $\mathbf{x}_s(t)$ is the vector of relative displacements with respect to the base, $\mathbf{x}_b(t)$ is the vector of base displacements, $\ddot{\mathbf{x}}_g(t)$ is the excitation vector, and $\mathbf{M}_s, \mathbf{C}_s, \mathbf{K}_s$, and $\mathbf{G}_s$ are the corresponding mass, damping, stiffness and earthquake influence coefficients matrices, respectively. On the other hand, the equation of motion of the base platform can be written as

$$(\mathbf{G}_s^T\mathbf{M}_s\mathbf{G}_s + \mathbf{M}_b)(\ddot{\mathbf{x}}_b(t) + \ddot{\mathbf{x}}_g(t)) + \mathbf{G}_s^T\mathbf{M}_s\ddot{\mathbf{x}}_s(t) + \mathbf{C}_b\dot{\mathbf{x}}_b(t) + \mathbf{K}_b\mathbf{x}_b(t) + \mathbf{f}_{is}(t) = \mathbf{0}, \tag{34}$$

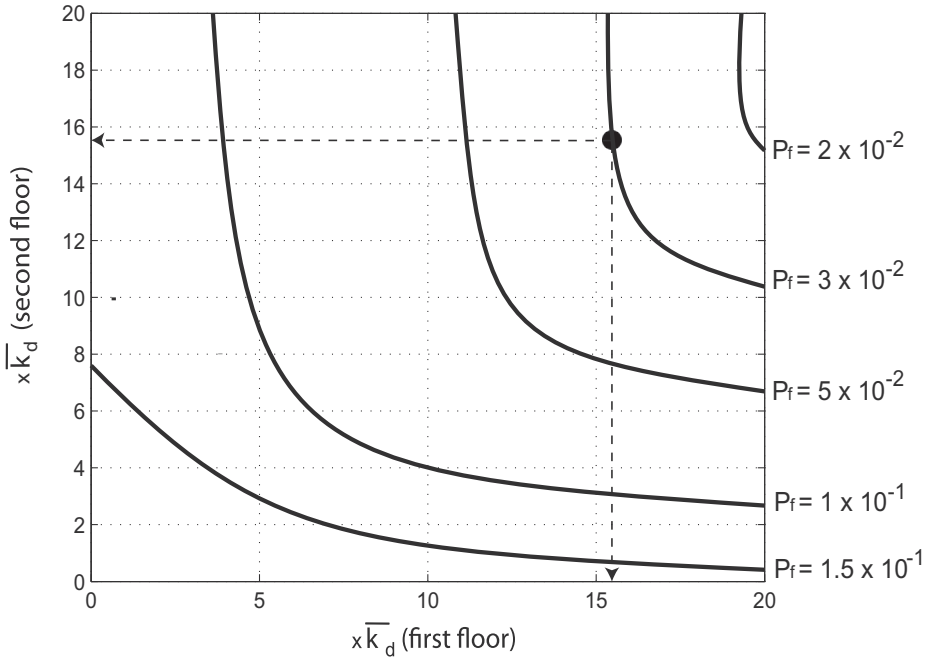


**Fig. 14.** Iso-probability curves corresponding to the system with prior uncertainties in terms of the initial stiffness of the hysteretic devices.

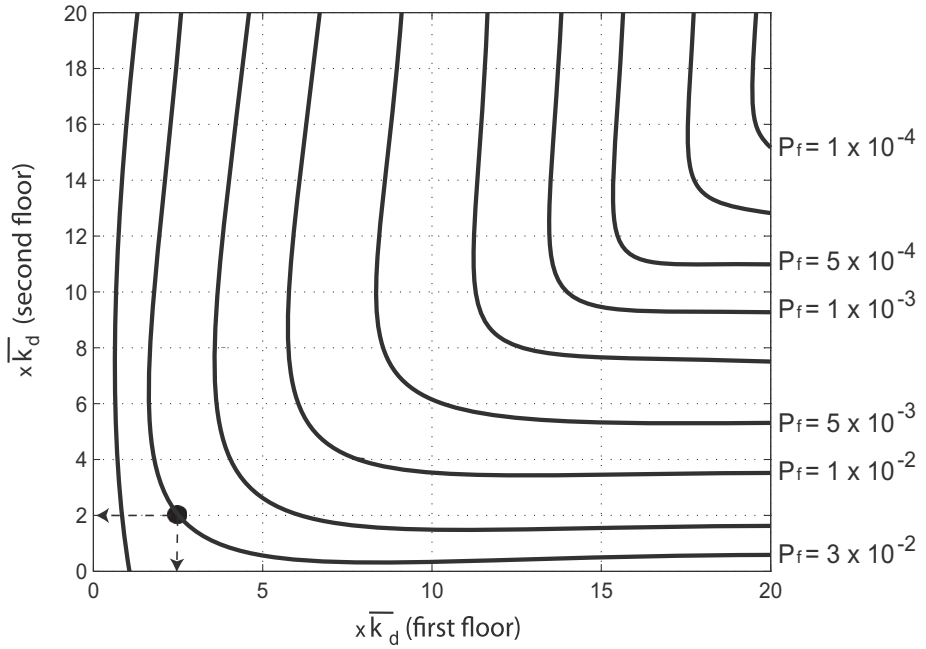


**Fig. 15.** Iso-probability curves corresponding to the updated system in terms of the initial stiffness of the hysteretic devices.

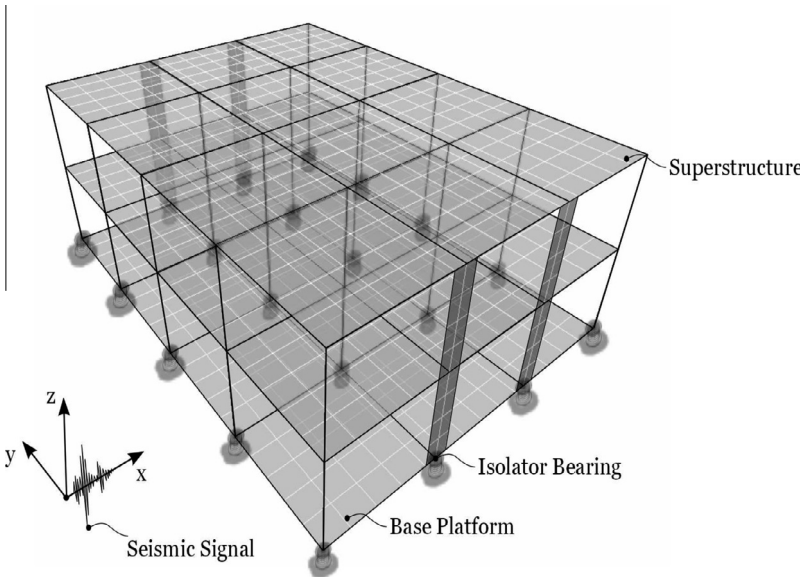


**Fig. 16.** Building model with base isolation system.

where $\mathbf{M}_b$ is the mass matrix of the rigid base, $\mathbf{C}_b$ is the resultant damping matrix of viscous isolation components, $\mathbf{K}_b$ is the resultant stiffness matrix of elastic isolation components, and $\mathbf{f}_{is}(t)$ is the vector containing the non-linear isolation element forces. In the previous equations it has been assumed that the superstructure remains elastic and the base platform is rigid in plane. Rewriting the previous equations, the combined equation of motion of the base-isolated structural system can be formulated in the form

$$\begin{bmatrix} \mathbf{M}_s & \mathbf{M}_s\mathbf{G}_s \\ \mathbf{G}_s^T\mathbf{M}_s & \mathbf{M}_b + \mathbf{G}_s^T\mathbf{M}_s\mathbf{G}_s \end{bmatrix} \begin{Bmatrix} \ddot{\mathbf{x}}_s(t) \\ \ddot{\mathbf{x}}_b(t) \end{Bmatrix} + \begin{bmatrix} \mathbf{C}_s & \mathbf{O} \\ \mathbf{O} & \mathbf{C}_b \end{bmatrix} \begin{Bmatrix} \dot{\mathbf{x}}_s(t) \\ \dot{\mathbf{x}}_b(t) \end{Bmatrix} + \begin{bmatrix} \mathbf{K}_s & \mathbf{O} \\ \mathbf{O} & \mathbf{K}_b \end{bmatrix} \begin{Bmatrix} \mathbf{x}_s(t) \\ \mathbf{x}_b(t) \end{Bmatrix} = -\begin{bmatrix} \mathbf{M}_s\mathbf{G}_s \\ \mathbf{M}_b + \mathbf{G}_s^T\mathbf{M}_s\mathbf{G}_s \end{bmatrix} \ddot{\mathbf{x}}_g(t) - \begin{Bmatrix} \mathbf{0} \\ \mathbf{f}_{is}(t) \end{Bmatrix}. \tag{35}$$

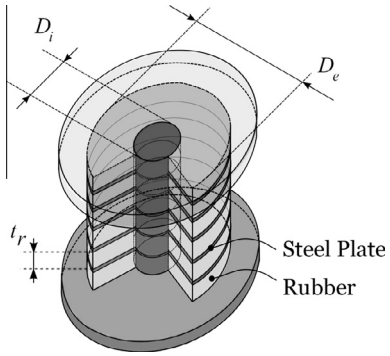


**Fig. 17.** Schematic representation of a rubber bearing.

Note that the combined equation of motion (superstructure and isolation system) constitutes a nonlinear system of equations due to the nonlinearity of the isolation forces (see next Section). The solution of the equation of motion (35) is obtained in an iterative manner by using any suitable step-by-step nonlinear integration scheme. From the numerical implementation point of view the diaphragms in the finite element model are assumed to be rigid in plane. Then using kinematic relationships and condensation techniques nine master degrees of freedom are finally defined, which are the ones used in the dynamic analysis.

*5.3.3. Isolation system model class*

An analytical model that simulates measured restoring forces under bidirectional loadings is used in the present application. The model is based on a series of experimental tests conducted for real-sized rubber bearings [50]. On the basis of the test results the model assumes that the restoring force on the rubber bearing is composed of a force directed to the origin of the isolator and another force approximately opposite to the direction of the movement of the isolator. The direction of the movement $\mathbf{d}(t)$ is defined in terms of the base displacement vector $\mathbf{x}(t)$ (components in the $x$ and $y$ direction of $\mathbf{x}_b(t)$) by means of the nonlinear differential equation [50]

$$\dot{\mathbf{d}}(t) = \frac{1}{\alpha}\|\dot{\mathbf{x}}(t)\|\left[\hat{\dot{\mathbf{x}}}(t) - \|\mathbf{d}(t)\|^n \hat{\mathbf{d}}(t)\right], \quad \mathbf{x}(0) = \mathbf{0}, \quad \mathbf{d}(0) = \mathbf{0}, \tag{36}$$

where $\dot{\mathbf{x}}(t)$ is the velocity vector, $\hat{\dot{\mathbf{x}}}(t)$ and $\hat{\mathbf{d}}(t)$ are the unit directional vectors of $\dot{\mathbf{x}}(t)$ and $\mathbf{d}(t)$, respectively, and $\|\cdot\|$ indicates the Euclidean norm. The parameters $\alpha$ and $n$ are positive constants that relate to the yield displacement and smoothness of yielding, respectively. Once the vector $\mathbf{d}(t)$ has been derived, the restoring force on each of the isolators is expressed in terms of the unit directional vector $\dot{\mathbf{x}}(t)$ and the vector $\mathbf{d}(t)$ as $\mathbf{f}(t) = -\hat{\dot{\mathbf{x}}}(t)f_e(t) - \mathbf{d}(t)f_s(t)$, where $f_e(t)$ is the non-linear elastic component and $f_s(t)$ is the elastoplastic component. Based on experimental results, the non-linear elastic component can be approximated as $f_e(t) = A\, s_2(\gamma(t))$, where $A = \pi/4(D_e^2 - D_i^2)$ is the cross sectional area of the rubber and $s_2(\cdot)$ is a quadratic polynomial in terms of the average shear stress $\gamma(t) = \|\mathbf{x}(t)\|/H_r$. On the other hand, the elastoplastic-plastic component can be expressed as $f_s(t) = A\, s_3(\gamma(t))$ where $s_3(\cdot)$ is a cubic polynomial in terms of the average shear stress $\gamma(t)$ [50,51]. Similarly, the parameters $\alpha$ and $n$ can be calibrated from the experimental data. The estimated values are $\alpha = 0.25H_r$ and $n = 0.7$. Validation calculations have shown that the analytical model is able to accurately simulate the test results for both bidirectional and unidirectional loading [50]. Based on the previous analytical model, the isolation system model class is defined in terms of the external diameter of the isolator and the total height of rubber in the device. These parameters are parameterized as $D_e = \theta_1 \bar{D}_e$ and $H_r = \theta_2 \bar{H}_r$, where $\bar{D}_e$ and $\bar{H}_r$ are the corresponding nominal values.

*5.3.4. Identification of isolator parameters*

As in the previous applications, it is assumed that the base-isolated structural system is built and response data are available to update the isolation model. The model updating is based on measurements of the ground acceleration at the support of the isolation system and of the absolute acceleration response in the $x$ direction at the base platform. The actual base-isolated system used to generate the simulated measured data corresponds to the structural model previously described with isolator parameters $D_e = 0.75$ m, $H_r = 0.20$ m, and $D_i = 0.10$ m. This isolation system is more flexible than the nominal one indicating that the isolator properties have changed due to, for example, large shear strains developed in the devices during a severe earthquake. The input ground acceleration history, applied in the $x$ axis, is taken as the one shown in Fig. 2. The measured response is simulated by first calculating the absolute base acceleration response and then adding 10% *rms* Gaussian white noise. Thirty seconds of data with sampling interval $\Delta t = 0.01$ s are used, given a total of $N_t = 3000$ data points. For illustration purposes Fig. 18 shows a typical displacement-restoring force curve of one of the isolators. The nonlinear incursion is clear from the figure.

For the identification process independent uniform prior distributions are assumed for the parameters $\theta_1$ and $\theta_2$ over the range $[0.7, 1.5]$. Note that these parameters affect the nonlinear behavior of the isolators. Therefore the identification process in this case is related to parameters that control the nonlinear response of the isolation system. The number of samples at the

different iteration steps of the transitional Markov chain Monte Carlo method is taken as 1000, that is $N_j = 1000, j = 1, \ldots, m$, while the scaling parameters are equal to 0.04. The samples from the prior and the posterior probability density functions are displayed in terms of the parameters $\theta_1$ and $\theta_2$ in Fig. 19A and B, respectively. The value of the nominal model parameters is also indicated in the figure. In this application the number of model evaluations required for performing the identification process is equal to 6000. The large prior uncertainty about the isolator parameters $(D_e, H_r)$ is reduced which is visible from the decreased range of the posterior samples. The samples of the external diameter are distributed around the actual value of 0.75 m ($\theta_1 = 0.89$) as shown in the corresponding histogram of this parameter (Fig. 20). On the other hand, it is observed from Fig. 19B that the total height of rubber in the device is essentially unidentifiable to a unique value with the provided data. This result is reasonable since numerical validations have shown that the response of the base platform is relatively insensitive to this parameter over the range considered (12 cm $\leqslant H_r \leqslant$ 25 cm) [51]. Thus, no unique solution can be identified in this case. The results of Fig. 19B also suggest that the data for the updated model result in uncertainties that are correlated along a certain direction. The correlation structure is consistent with the fact that the base isolation system becomes stiffer as the rubber diameter is increased. Contrarily, the isolation system becomes more flexible as the height of the rubber is increased. Therefore, an increase in the rubber diameter is compensated by an increase in the height of the rubber during the updating process, and all points along that direction correspond to isolation system models that have similar base drift responses. The previous results illustrate some of the advantages of Bayesian updating procedures over traditional techniques that try to identify one best model when there is limited amount of data available. In this case the identification problem emerges as ill-conditioned without a unique solution which can be tackled very efficiently by Bayesian model updating.

### 5.3.5. Base-isolation performance

The performance of the base isolation system is evaluated in terms of the probability of a failure event associated with the base drift response. This response together with the interstory drifts and absolute accelerations of the superstructure are usually the quantities to be controlled during the design of base-isolation systems. The failure domain related to the base drift is defined as

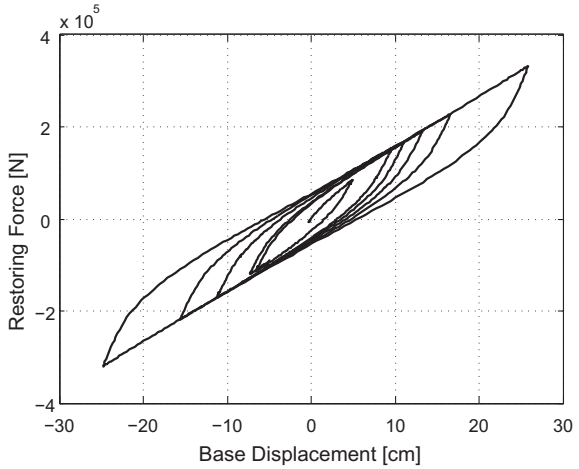


**Fig. 18.** Typical displacement-restoring force curve of one of the isolators.

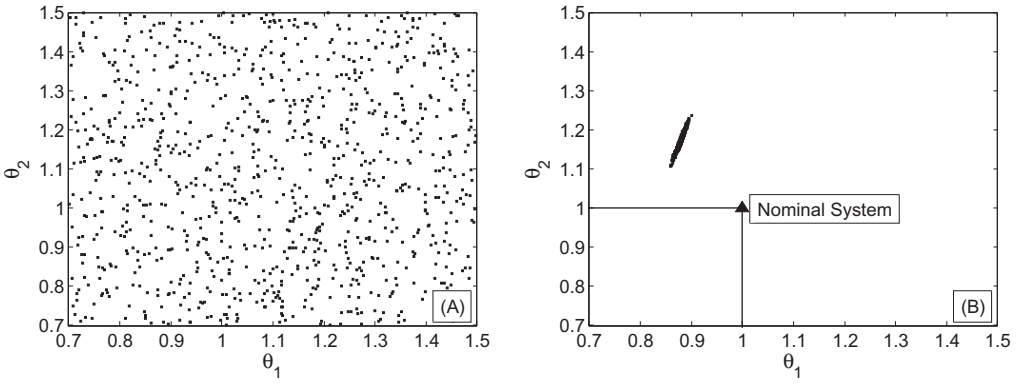


**Fig. 19.** Samples of the prior (A) and posterior (B) probability density functions of the parameters $\theta_1$ and $\theta_2$.

$$F(M) = \left\{ \mathbf{q}^T =< \mathbf{z}^T, \boldsymbol{\theta}^T > | d(\mathbf{q}|M) = \max_{t\in[0,T]} \frac{|x_{b_x}(t,\mathbf{z},\boldsymbol{\theta})|}{x^*_{b_x}} > 1 \right\}, \tag{37}$$

where $\mathbf{q}$ represents the augmented vector of system parameters, $x_{b_x}(t,\mathbf{z},\boldsymbol{\theta})$ represents the base displacement in the $x$ direction, and $x^*_{b_x} = 25$ cm is the corresponding threshold level. In what follows the effect of monitoring data and parametric uncertainty on the reliability of the isolation system is considered. To this end the probability of failure of the nominal and updated systems are compared. Recall that the nominal system may be considered as the pre-test model used in the design stage of the isolation system. As in the previous application problems the estimation of the failure probabilities represents a high-dimensional reliability problem.

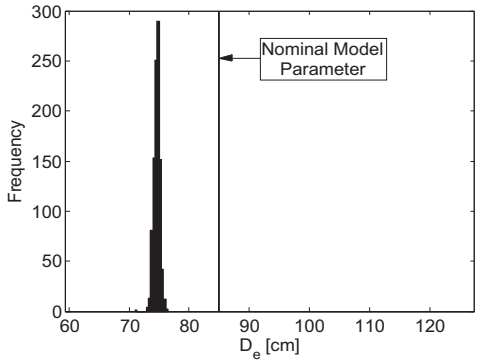


**Fig. 20.** Histogram of the external diameter samples.

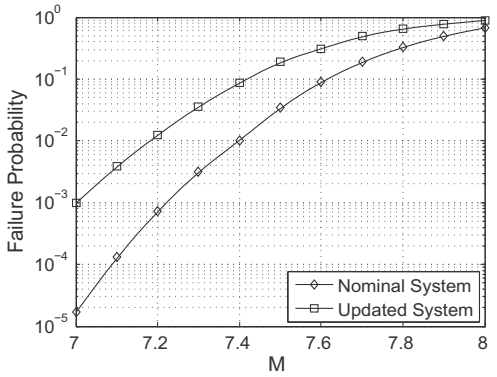


**Fig. 21.** Failure probability of the nominal and updated systems in terms of the moment magnitude $M$.

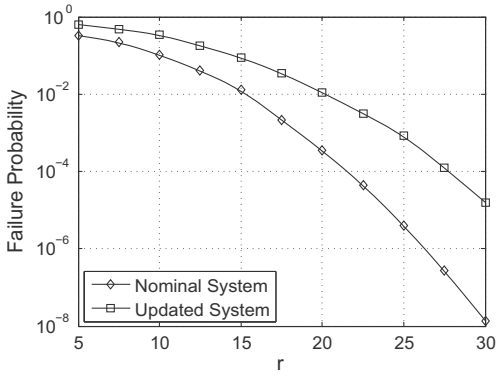


**Fig. 22.** Failure probability of the nominal and updated systems in terms of the epicentral distance $r$.

The failure probability of the nominal and updated systems in terms of the moment magnitude $M$ is shown in Fig. 21. A range between 7.0 and 8.0 is considered for moment magnitude. The epicentral distance is fixed at 15 km. It is seen that the probability of failure increases for both systems as the moment magnitude increases as expected. On the other hand, the failure probability of the nominal and updated systems in terms of the epicentral distance $r$ is presented in Fig. 22. In this case the moment magnitude is fixed at 7.2 and a range between 5.0 km and 30 km is considered for the epicentral distance. As anticipated, the probability of failure decreases for both systems as the epicentral distance increases. From these figures it is observed that the failure probability of the updated system (updated robust failure probability) is larger than the corresponding to the nominal system. It is also seen that the difference is significant in some cases (more than one order of magnitude). The differences are caused by the uncertainties in the model parameters inferred from the test data by the Bayesian formulation and from the fact that the isolation devices in the updated model are more flexible. The number of analyses involved in the estimation of the updated failure probabilities shown in Figs. 21 and 22 varies between 2000 and 11,000, depending on the value of the failure probability. The previous results show, once again, the importance of using dynamic data, whenever available, in order to obtain a more accurate picture of the system performance.

## 6. Conclusion

The use of updated robust reliability measures in the context of stochastic structural dynamical systems has been explored. A simulation-based Bayesian framework for system identification is used to update the structural models using dynamic response data. The updated distribution of the system model parameters is then used to implement a methodology for estimating the system reliability which incorporates knowledge from the test data. The estimates obtained by the proposed scheme are similar to the ones obtained directly from the samples generated during the identification process. However, the proposed implementation reduces the computational cost by one or two orders of magnitude. Numerical results show that the structural reliability computed before and after using dynamic data can differ significantly. In fact, monitoring data and the resulting modeling uncertainties makes an important difference in the performance evaluation and design of structural systems. Therefore, measured responses, whenever available, should be used. In this manner a more accurate description of the system performance and reliability can be obtained. Future research efforts aim at expanding the study reported herein. Specific issues to be investigated include: the application of the proposed implementation to larger FE models and more general nonlinear models; the parallelization of the updating reliability scheme; and the implementation of surrogate approximation schemes for evaluating system responses in the context of dynamical systems under stochastic excitation.

## Acknowledgments

The research reported here was supported in part by CONICYT under Grant No. 1110061 which is gratefully acknowledged by the authors. Also this research has been implemented under the "ARISTEIA" Action of the "Operational Programme Education and Lifelong Learning" and was co-funded by the European Social Fund (ESF) and Greek National Resources.

## References

[1] H.O. Madsen, Model updating in reliability theory, in: Proc. ICASP 5, Vancuver, Canada, 1987.
[2] M. Fujita, R. Rackwitz, Updating first and second order reliability estimates by importance sampling, Proc. JSCE, Struct. Engrg./Earthquake Engrg. 5 (1) (1988) 53–59.
[3] Z. Zhao, A. Haldar, F.L. Breen, Fatigue-reliability updating through inspection of steel bridges, J. Struct. Engrg. ASCE 120 (5) (1994) 1624–1641.
[4] R. Sindel, R. Rackwitz, Problems and solution strategies in reliability updating, J. Offshore Mech. Arct. Engrg 120 (2) (1998) 109–114.
[5] J.T.P. Yao, H.G. Natke, Damage detection and reliability evaluation of existing structures, Struct. Saf. 15 (1994) 3–16.
[6] G. Deodatis, H. Asada, S. Ito, Reliability of aircraft structures under nonperiodic inspection – a Bayesian approach, J. Engrg. Fract. Mech. 53 (5) (1996) 789–805.
[7] C. Cremona, Reliability updating of welded joints damaged by fatigue, Int. J. Fatigue 18 (1996) 567–575.
[8] H. Shoji, M. Shinozuka, S. Sampath, A Bayesian evaluation of simulation models of multiple-site fatigue crack, Probab. Engrg. Mech. 16 (2001) 355–361.
[9] P. Beaurepaire, M.A. Valdebenito, G.I. Schuëller, H.A. Jensen, Reliability-based optimization of maintenance scheduling of mechanical components under fatigue, Comput. Methods Appl. Mech. Engrg. 221-222 (2012) 24–40.
[10] C. Papadimitriou, J.L. Beck, L. Katafygiotis, Updating robust reliability using structural test data, Probab. Engrg. Mech. 16 (2001) 103–113.
[11] J.L. Beck, S.K. Au, Bayesian updating of structural models and reliability using Markov chain Monte Carlo simulation, J. Engrg. Mech. 128 (4) (2002) 380–391.
[12] J.L. Beck, Bayesian system identification based on probability logic, Struct. Control Health Monit. 17 (7) (2010) 825–847.
[13] K.V. Yuen, Bayesian Methods for Structural Dynamics and Civil Engineering, John Wiley & Sons, 2010.
[14] J. Ching, Y.C. Chen, Transitional Markov chain Monte Carlo method for Bayesian updating, model class selection and model averaging, J. Engrg. Mech. 133 (2007) 816–832.
[15] G.E. Box, G.C. Tiao, Bayesian Inference in Statistical Analysis, Wiley, New York, 1992.
[16] A.B. Mason, W.D. Iwan, An approach to the first passage problem in random vibration, J. Appl. Mech. ASME 50 (1983) 641–646.
[17] A. Naess, Approximate first-passage and extremes of narrow-band Gaussian and non-Gaussian random vibrations, J. Sound Vib. 5138 (3) (1990) 365–380.
[18] L.D. Lutes, S. Sarkani, Random Vibrations: Analysis of Structural and Mechanical Systems, Elsevier B-H, Oxford, UK, 2004.
[19] N. Metropolis, A. Resenbluth, M. Resenbluth, A. Teller, E. Teller, Equations of state calculations by fast computing machines, J. Chem. Phys. 21 (6) (1953) 1087–1092.
[20] W. Hastings, Monte Carlo sampling methods using Markov chains and their applications, Biometrika 57 (1) (1970) 97–109.
[21] J. Beck, L. Katafygiotis, Updating models and their uncertainties. I: Bayesian statistical framework, J. Engrg. Mech. 124 (4) (1998) 455–461.

[22] L. Katafygiotis, J. Beck, Updating models and their uncertainties. II: model identifiability, J. Engrg. Mech. 124 (4) (1998) 463–467.
[23] K.V. Yuen, S.C. Kuok, Bayesian methods for updating dynamic models, Appl. Mech. Rev. 64 (1) (2011) 010802-1–010802-18.
[24] H. Jeffreys, Theory of Probability, third ed., Oxford University Press, USA, 1961.
[25] J.L. Beck, K.V. Yuen, Model selection using response measurements: Bayesian probabilistic approach, J. Engrg. Mech. 130 (2) (2004) 192–203.
[26] E. Jaynes, Probability Theory: The Logic of Science, Cambridge University Press, 2003.
[27] F.E. Udwadia, Some uniqueness related to soil and building structural identification, SIAM J. Appl. Mech. 45 (1985) 674–685.
[28] L. Katafygiotis, Treatmenmt of model uncertainties in structural dynamics, Technical Report EERL91-01, California Institute of Technology, Pasadena, CA. 1991.
[29] C.M. Yang, J.L. Beck, Generalized trajectory methods for finding multiple extrema and roots of functions, J. Optim. Theor. Appl. 97 (4) (1998) 211–227.
[30] L.S. Katafygiotis, C. Papadimitriou, H.F. Lam, A probabilistic approach to structural model updating, J. Soil Dyn. Earthquake Engrg. 17 (1998) 495–507.
[31] L.S. Katafygiotis, H.F. Lam, C. Papadimitriou, Treatment of unidentifiability in structural model updating, Adv. Struct. Engrg. 3 (1) (2000) 19–39.
[32] N. Bleistein, R. Handelsman, Asymptotic Expansions for Integrals, Dover Publicactions, Inc., New York, 1986.
[33] B. Goller, J.L. Beck, G.I. Schuëller, Evidence-based identification of weighting factors in Bayesian model updating using modal data, in: ECCOMAS Thematic Conference on Computational Methods in Structural Dynamics and Earthquake Engineering, Rhodes, Greece, 2009.
[34] B. Goller, M. Broggi, A. Calvi, G.I. Schuëller, A stochastic model updating technique for complex aerospace structures, Finite Elem. Anal. Des. 47 (2011) 739–752.
[35] P. Angelikopoulos, C. Papadimitriou, P. Koumoutsakos, Bayesian uncertainty quantification and propagation in molecular dynamics simulations: a high performance computing framework, J. Chem. Phys. 137 (2012). 144103-1, 144103-19.
[36] T. Soong, M. Grigori, Random Vibration of Mechanical and Structural Systems, Printece Hall, Englewood Cliffs, NJ, 1993.
[37] R.M. Neal, Estimating ratios of normalizing constants using linked importance sampling. Technical Report No. 0511, Department of Statistics, University of Toronto, 2005
[38] H.J. Pradlwarter, G.I. Schuëller, P.S. Koutsourelakis, D.C. Charmpis, Application of line sampling simulation method to reliability benchmark problems, Struct. Saf. 29 (3) (2007) 208–221.
[39] S.K. Au, J.L. Beck, First excursion probabilities for linear systems by very efficient importance sampling, Probab. Engrg. Mech. 16 (3) (2001) 193–207.
[40] S.K. Au, J.L. Beck, Estimation of small failure probabilities in high dimensions by subset simulation, Probab. Engrg. Mech. 16 (4) (2001) 263–277.
[41] J. Ching, S.K. Au, J.L. Beck, Reliability estimation for dynamical systems subject to stochastic excitation using subset simulation with splitting, Comput. Methods Appl. Mech. Engrg. 194 (12-16) (2005) 1557–1579.
[42] A. Gelman, G.O. Roberts, W.R. Gilks, Efficient Metropolis jumping rules, Bayesian Stat. 5 (1996) 599–607.
[43] K. Zuev, J.L. Beck, S.K. Au, L. Katafygiotis, Bayesian post-processor and other enhancements of subset simulation for estimating failure probabilities in high dimensions, Comput. Struct. 5 (2011) 599–607.
[44] R. Clough, J. Penzien, Dynamics of Structures, McGraw-Hill, New York, 1975.
[45] H.A. Jensen, M.A. Valdebenito, G.I. Schuëller, D.S. Kusanovic, Reliability-based optimization of Stochastic systems using line search, Comput. Methods Appl. Mech. Engrg. 198 (49-52) (2009) 3915–3924.
[46] G.M. Atkinson, W. Silva, Stochastic modeling of California ground motions, Bull. Seismol. Soc. Am. 90 (2) (2000) 255–274.
[47] D.M. Boore, Simulation of ground motion using the Stochastic method, Pure Appl. Geophys. 160 (3-4) (2003) 635–676.
[48] J.G. Anderson, S.E. Hough, A model for the shape of fhe Fourier amplitude spectrum of acceleration at high frequencies, Bull. Seismol. Soc. Am. 74 (5) (1984) 1969–1993.
[49] D.M. Boore, W.B. Joyner, T.E. Fumal, Equations for estimating horizontal response spectra and peak acceleration from western north american earthquakes: a summary of recent work, Seismol. Res. Lett. 68 (1) (1997) 128–153.
[50] M. Yamamoto, S. Minewaki, H. Yoneda, M. Higashimo, Nonlinear behavior of high-damping rubber bearings under horizontal bidirectional loading: full-scale tests and analytical modeling, Earthquake Engrg. Struct. Dyn. 41 (13) (2012) 1845–1860.
[51] H.A. Jensen, D.S Kusanovic, M. Papadrakakis, Reliability-based characterization of base-isolated structural systems, European Congress on Computational Methods in Applied Sciences and Engineering, Vienna, Austria, 2012.